Pergamon

PII S0016-7037(00)01004-9

Geochemistry of xenolithic eclogites from West Africa, part 2: Origins of the high MgO eclogites

Matthias G. Barth,[1,*] Roberta L. Rudnick,[1,†] Ingo Horn,[1,‡] William F. McDonough,[1,†] Michael J. Spicuzza,[2]
John W. Valley,[2] and Stephen E. Haggerty[3,§]

[1]Department of Earth and Planetary Sciences, Harvard University, 20 Oxford Street, Cambridge, MA 02138, USA
[2]Department of Geology and Geophysics, University of Wisconsin, 1215 W Dayton Street, Madison, WI 53706, USA
[3]Department of Geosciences, University of Massachusetts, Morrill Science Center, Amherst, MA 01003, USA

Abstract—Oxygen isotope, mineral trace element, and measured and reconstructed whole-rock compositions are reported for the high MgO eclogite xenolith suite (16 to 20 wt% MgO in the whole rock) from the Koidu Kimberlite complex, Sierra Leone. In contrast to the previously published data for low MgO eclogites (6 to 13 wt% MgO) from this area, high MgO eclogites equilibrated at higher temperatures (1080 to 1130°C vs. 890 to 930°C) have only mantlelike $\delta^{18}O$ and show variable degrees of light rare earth element (REE) enrichment. Analyses of multiple mineral generations suggest that the heterogeneous REE patterns of the high MgO eclogites reflect variable degrees of metasomatic overprinting. High MgO and Al_2O_3 contents of the eclogites suggest a cumulate origin, either as high-pressure (2 to 3 GPa) garnet–pyroxene cumulates or low-pressure (<1 GPa) plagioclase–pyroxene–olivine cumulates. Trace element modeling suggests a low-P origin for eclogites with flat heavy REE patterns and a high-P origin for eclogites with fractionated heavy REE. Flat heavy REE patterns, the presence of Sr anomalies, and low to moderate transition element contents in the low-P group are consistent with a low-pressure origin as metamorphosed olivine gabbros and troctolites. These metagabbroic high MgO eclogites either could represent the basal section of subducted oceanic crust or foundered mafic lower continental crust. In the former case, the metagabbroic high MgO eclogites may be genetically related to the Koidu low MgO suite. Crystal fractionation trends suggest that the metapyroxenitic high MgO eclogites formed at lower pressures than their current estimated equilibrium pressures (>4 GPa). *Copyright © 2002 Elsevier Science Ltd*

1. INTRODUCTION

Eclogites that occur as xenoliths in kimberlites have been variably interpreted as formed as cumulates that crystallized in situ from peridotite-generated magmas ("mantle" hypothesis) (MacGregor and Carter, 1970; Smyth et al., 1989; Caporuscio and Smyth, 1990) or that formed via prograde metamorphism of subducted basaltic oceanic crust, which may or may not have lost a melt component associated with subduction (the "crustal" hypothesis; Helmstaedt and Doig, 1975; MacGregor and Manton, 1986; Taylor and Neal, 1989; Ireland et al., 1994; Jacob et al., 1994; Schulze et al., 1997, 2000; Barth et al., 2001). A variant of the crustal hypothesis that has not been widely explored is that eclogites may be products of metamorphism of mafic lower continental crust—that is, products of isobaric cooling at high pressure of gabbroic to anorthositic protoliths (Griffin et al., 1990; El Fadili and Demaiffe, 1999).

In contrast to most other kimberlite occurrences, eclogites dominate the mantle xenolith population at the Koidu kimberlite complex in Sierra Leone, West Africa. Here, the eclogites fall into two groups, which are based on distinct major element

and mineral chemistry (Fig. 1; Hills and Haggerty, 1989; Fung and Haggerty, 1995): a high MgO group (>16 wt% MgO in the whole rock) and a low MgO group (6 to 13 wt% MgO). This article is the second that examines oxygen isotope and trace element characteristics of these eclogites. The first article (Barth et al., 2001) reports the oxygen isotopic compositions and the trace element compositions of the low MgO eclogites. These data showed that the low MgO group are depleted in light rare earth elements (LREEs) and have $\delta^{18}O$ that both overlap with and range beyond mantle $\delta^{18}O$ values. We interpreted these results to reflect an origin of the low MgO eclogites as ancient altered oceanic crust that underwent an episode of partial melting during subduction (Barth et al., 2001), supporting previous suggestions that xenolithic eclogites may represent the residua left after formation of the Na-rich granites found in the vicinity of the Koidu kimberlites in the Archean Man Shield (Rollinson, 1997).

The high MgO eclogites from Koidu, although carried in the same kimberlite pipe, have distinctive petrographic, chemical, and petrologic features from the low MgO group. For this reason, and to limit the length of any given published work, we decided to treat these two suites in separate articles. In this article, we present the oxygen isotopic compositions, the trace element characteristics, and the genesis of the Koidu high MgO eclogites (Hills and Haggerty, 1989, Fung and Haggerty, 1995). We use these data to determine whether a genetic link exists between the low MgO and high MgO eclogite suites and to compare with other eclogite occurrences, both as xenoliths and in massifs, to provide further insight into the petrogenesis of eclogite in the upper mantle.

* Author to whom correspondence should be addressed (barth@geo.uu.nl).
† *Present address:* Department of Geology, University of Maryland, College Park, MD 20742, USA.
‡ *Present address:* Laboratory for Inorganic Chemistry, ETH Zürich, Universitätsstrasse 6, CH-8092 Zürich, Switzerland.
§ *Present address:* Department of Earth Sciences, Florida International University, University Park, PC344, 11200 SW 8th Street, Miami, FL 33199, USA
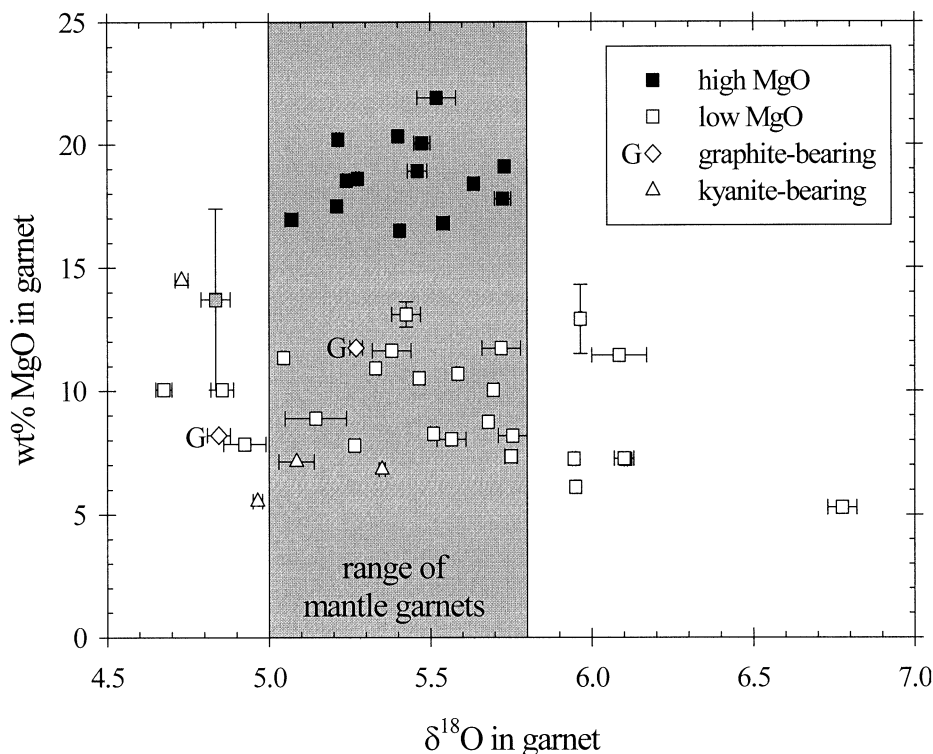
Fig. 1. MgO in garnet vs. $\delta^{18}O$ in garnet for Koidu eclogites. Solid squares represent high MgO eclogites; open symbols show low MgO eclogites (Barth et al., 2001). The gray square denotes the transitional eclogite KEC 86-19. Open squares = bimineralic eclogites; open diamonds = graphite-bearing eclogites; open triangles = kyanite-bearing eclogites. Horizontal error bars show average reproducibility (each wing is half of the difference between two separate measurements); vertical error bars indicate mineral zoning. The gray field depicts the range of mantle garnets that is shifted toward lighter isotopic composition by 0.1‰ relative to the whole-rock mantle range as a result of the fractionation between garnet and whole rock.

2. GEOLOGICAL BACKGROUND

The Koidu Kimberlite Complex, located on the Man Shield of the West African Craton, consists of three Mesozoic kimberlite pipes, a ring-dike structure, and multiple sets of en echelon kimberlite dikes. The surrounding country rocks comprise various members of an Archean basement assemblage composed of migmatites, syntectonic granites, banded ironstones, and metamorphosed ultramafic suites (Hurley et al., 1975; Rollinson, 1978, 1982; MacFarlane et al., 1981). The mantle xenolith suite is dominated by eclogites, with discrete garnet, pyroxene, ilmenite, and ilmenite–pyroxene intergrowths being less abundant (Tompkins and Haggerty, 1984). Although peridotite xenoliths are apparently absent, peridotite suite diamonds are recorded (Harris and Gurney, 1979).

Hills and Haggerty (1989) and Fung and Haggerty (1995) describe the petrography and report mineral chemical data for 87 eclogite xenoliths and whole-rock X-ray fluorescence major and trace element data for 25 of these samples from Pipe Number 1 at Koidu. The eclogites are coarse-grained and equigranular, and they have garnet-to-pyroxene modal ratios typically ranging between 40:60 and 60:40. The high MgO group (>16 wt% MgO) is essentially bimineralic, with only minor ilmenite, sulfide, or both occurring in addition to garnet and omphacite. The low MgO group (6 to 13 wt% MgO) commonly contains accessory phases such as kyanite, graphite,

quartz (after coesite), diamond, amphibole, corundum plus rutile, or sulfides in addition to garnet and omphacite. High MgO garnets fall within the field of group A eclogites as defined by Coleman et al. (1965); the low MgO garnets occupy the group B and C eclogite regions. Generally, both high and low MgO eclogites fall into the classification of group II eclogites of McCandless and Gurney (1989)—that is, low Na garnets and low K omphacite, except for the diamond-bearing eclogites and a single graphite-bearing eclogite that fall into group I.

The Koidu eclogites show a large range of textures, estimated equilibration temperatures, and pressures, extending from 760°C at 2.8 GPa to 1188°C at 5 GPa (using the Ellis and Green, 1979, geothermometer and a representative cratonic geotherm—the Kalahari geotherm of Rudnick and Nyblade, 1999). The P-T ranges of the high and low MgO eclogites differ significantly (Hills and Haggerty, 1989; Fung and Haggerty, 1995); many high MgO eclogites record conditions between 1080 to 1130°C and 4.0 to 4.5 GPa, whereas the low MgO eclogites cluster between 880 to 930°C and 3.3 to 3.6 GPa.

3. ANALYTICAL METHODS

Mineral separates for laser fluorination oxygen isotope ratio analysis were prepared by standard procedures including initial crushing in alumina ceramics followed by magnetic separation. Purity of samples

Table 1. Oxygen isotopic composition of Koidu high MgO eclogite garnet separates determined by laser fluorination (all samples have KEC prefix).[a]

Sample	$\delta^{18}O_{SMOW}$	1σ	Jadeite in cpx (mol%)
KEC 80-B1	5.73	0.03	12
KEC 81-2	5.54	0.02	13
KEC 81-11	5.52	0.06	16
KEC 86-2	5.64	0.02	11
KEC 86-8	5.48	0.03	11
KEC 86-15	5.21	0.00	21
KEC 86-60	5.24	0.01	13
KEC 86-73A	5.73	0.00	17
KEC 86-90	5.28	0.00	11
KEC 86-107	5.40	—	18
K91-6	5.07	0.02	22
K91-10	5.22	0.01	13
K91-16	5.41	0.00	12
K91-46	5.46	0.03	12
Transitional eclogite			
KEC 86-19	4.84	0.04	
Core			19
Rim			46

[a] All values of $\delta^{18}O$ are averages of two measurements except for KEC 86-107, which is a single measurement. 1σ is the average reproducibility, i.e., half of the difference between two separate measurements. Samples are corrected to garnet standard UWG-2 = 5.8‰ (Valley et al., 1995).

was ensured by hand picking, with sample weights for each analysis ranging between 1 and 3 mg. Oxygen isotope ratios were measured at the University of Wisconsin, Madison, by means of a laser-assisted fluorination technique described by Valley et al. (1995). This method provides high oxygen yields for refractory minerals like garnet. In most cases repeat analyses fall within 0.1 '89 of each other, demonstrating the good reproducibility of the technique and the purity of the mineral separates. Measured values were corrected ($\leq$0.1‰) on the basis of three to four analyses of garnet standard UWG-2 at the start of each day (Valley et al., 1995). Corrected values are reported relative to V-SMOW (Coplen, 1996).

Whole-rock trace element compositions were determined by inductively coupled plasma-mass spectrometry (ICP-MS) after digestion in Teflon bombs. Analyses were performed on a Fisons (VG Elemental) PQ II+ in pulse counting mode (three points per peak). Analytical details, standard data, and typical precision are reported in Barth et al. (2000). Trace element compositions of garnets, omphacites, and ilmenites were determined by laser ablation ICP-MS. Ablation is achieved by a 193-nm Ar-F excimer laser system with a pulse repetition rate of 10 Hz and pulse energy of 0.5 mJ (Horn et al., 2000). Analyses were performed in pulse counting mode (one point per peak). Analytical details and standard values are given in Barth et al. (2001).

4. RESULTS

4.1. Oxygen Isotopes

Garnet oxygen isotopic data were obtained for 15 high MgO eclogites (Fig. 1, Table 1). Garnet is usually the freshest phase in eclogite xenoliths, is more resistant to isotopic resetting than clinopyroxene (Deines and Haggerty, 2000), and shows a larger range in composition (e.g., FeO content) than clinopyroxene. Garnet analyses are representative of the whole-rock oxygen isotopic composition because the theoretical and observed high-temperature isotope fractionation between garnet and clinopyroxene is small (<0.4‰; Rosenbaum and Mattey, 1995; Kohn and Valley, 1998; Snyder et al., 1998), with garnet being

lighter, on average, than clinopyroxene (Jacob et al., 1994; Beard et al., 1996).

Unlike the low MgO eclogite group, the high MgO garnets have a restricted range of $\delta^{18}O$ values (5.07 to 5.73‰) that fall, with one exception, within the mantle range ($\delta^{18}O$ = 5.5 $\pm$ 0.4‰ based on xenolithic peridotites; Mattey et al., 1994; Fig. 1). Sample KEC 86-19 has $\delta^{18}O$ below the mantle range, and is unique within the entire Koidu suite in exhibiting strongly zoned garnets (iron-rich cores and magnesium-rich rims), two generations of coexisting clinopyroxene, and no ilmenite or rutile, which are present in most other high and low MgO eclogites, respectively (Hills and Haggerty, 1989). This sample was originally classified as a high MgO eclogite on the basis of its bulk rock MgO content (16.3 wt%), but both generations of clinopyroxene and the iron-rich garnet cores place it in the fields defined by low MgO eclogites. KEC 86-19 therefore is transitional between the high and low MgO groups.

4.2. Trace Element Mineral Chemistry

The trace element compositions of minerals (garnet, clinopyroxene, and ilmenite) from seven Koidu high MgO eclogites, determined by laser ablation ICP-MS, are presented in Tables 2 to 4. All samples show variable degrees of modal and rare cryptic metasomatism (see below). Therefore, care was taken to perform analyses on crack-free, unaltered areas of the minerals. The combination of the high-quality optical imaging capabilities of the Harvard laser ablation system and the time-resolved analysis of the ablation signals ensures that altered and/or metasomatized parts of the silicate minerals were recognized and excluded from the trace element analyses. As a result of the limited grain size and the opaque nature of ilmenite in the thick sections (~100 μm) analyzed, altered parts of the ilmenite grains could not always be avoided during analysis. However, these were easily distinguished by the presence of highly incompatible trace elements (e.g., Sr, Ba) and were excluded from the averages.

Garnets (Table 2) are LREE depleted with chondrite-normalized La contents (La_N) from 0.05 to 0.10 or below the detection limit (Fig. 2). All garnets, excluding the transitional sample KEC 86-19, have relatively flat heavy rare earth element (HREE) patterns with $(Dy/Yb)_N$ from 0.64 to 0.97, and have high HREE contents (Yb_N from 10–18). Transitional sample KEC 86-19 shows a positive slope in the HREE ($(Dy/Yb)_N$ = 0.45) and strongly enriched HREE (Yb_N = 85). Garnet from one sample (KEC 86-58) has a negative Eu anomaly (Eu/Eu* = 0.81), whereas garnet from another (KEC 86-15) has a positive Eu anomaly (Eu/Eu* = 1.15). All garnets show variable degrees of high field strength element (HFSE) depletions (Fig. 3), with Nb and Ta below the detection limit (0.3 to 0.03 ppm and 0.08 to 0.01 ppm for Nb and Ta, respectively, depending on the spot size) for all but three samples (KEC 80-B1, KEC 86-19, and KEC 86-107). The garnets show pronounced negative Ti anomalies but only slight depletions in Zr and Hf relative to Sm. The concentration of alkali and alkaline earth elements in garnet are generally very low (e.g., Sr $\leq$0.4 ppm) or are below the detection limit (e.g., Rb, Cs, Ba).

Clinopyroxenes (Table 3) have convex-upward REE patterns and are LREE-enriched and HREE depleted (Fig. 4). Clinopyroxene in two samples (KEC 86-58 and KEC 86-107) have

Table 2. Trace element composition of garnet determined by LA-ICP-MS.[a]

Sample spots	KEC 80-B1		KEC 81-2		KEC 86-15		KEC 86-19		KEC 86-58		KEC 86-73B		KEC 86-107	
	n = 9	1σ	n = 9	1σ	n = 7	1σ	n = 7	1σ	n = 7	1σ	n = 6	1σ	n = 4	1σ
Sc	62.2	1.6	62.1	5.0	54.2	4.5	75.7	6.8	92.9	5.5	82.7	7.4	76.5	2.9
V	143	11	156	18	83.9	15.2	129	7	200	21	134	26	262	18
Cr	1398	138	268	2	612	191	90.1	42.4	1206	48	3122	372	2041	161
Ni	15.5	3.3	22.3	0.2	15.3	1.7	36.9	2.9	<50		71.4	—	24.9	3.2
Ga	ND		ND		ND		ND		10.5	0.9	ND		ND	
Rb	< 0.2		< 0.2		< 0.3		< 0.3		< 1.4		< 0.9		< 0.2	
Sr	< 0.2		0.16	—	0.07	—	0.36	0.14	< 0.3		< 0.3		0.26	0.06
Y	28.7	1.6	22.0	0.8	19.1	1.2	87.9	29.5	26.7	1.5	25.7	1.1	20.1	1.6
Zr	15.7	1.2	11.5	0.7	7.99	0.65	28.4	8.9	8.87	1.48	12.1	1.1	21.2	0.8
Nb	< 0.1		< 0.4		< 0.1		0.23	0.03	< 1.1		< 0.5		0.31	0.14
La	< 0.03		0.015	0.002	< 0.03		< 0.03		< 0.1		< 0.2		0.031	0.012
Ce	0.037	0.006	0.12	0.02	0.034	0.014	0.16	0.04	0.08	0.02	0.090	0.002	0.20	0.05
Pr	< 0.05		ND		< 0.02		ND		ND		ND		0.06	0.02
Nd	0.30	0.05	0.50	0.03	0.23	0.03	0.83	0.13	0.35	0.03	0.52	0.09	0.64	0.10
Sm	0.61	0.09	0.72	0.20	0.36	0.03	0.97	0.10	0.49	0.07	0.70	0.11	0.60	0.06
Eu	0.39	0.04	0.40	0.06	0.28	0.01	0.53	0.03	0.22	0.02	0.33	0.04	0.34	0.04
Gd	2.20	0.25	2.07	0.17	1.47	0.18	3.00	0.35	1.43	0.13	1.60	0.23	1.70	0.07
Tb	0.55	0.04	ND		0.37	0.02	ND		ND		ND		0.45	0.04
Dy	4.75	0.23	3.69	0.33	3.14	0.18	11.33	3.67	3.75	0.31	3.81	0.22	3.60	0.30
Ho	1.11	0.07	0.87	0.04	0.76	0.06	ND		ND		ND		0.85	0.04
Er	3.56	0.23	2.78	0.16	2.35	0.23	13.97	3.62	3.40	0.31	2.96	0.16	2.83	0.24
Tm	0.51	0.04	ND		0.34	0.03	ND		ND		ND		0.39	0.02
Yb	3.47	0.32	2.73	0.18	2.11	0.19	17.85	2.87	3.78	0.34	3.19	0.17	2.70	0.14
Lu	0.58	0.07	0.45	0.04	0.33	0.03	2.93	0.38	0.63	0.07	0.47	0.01	0.43	0.04
Hf	0.22	0.03	0.26	0.02	0.13	0.02	0.48	0.16	0.20	0.04	0.19	0.01	0.57	0.03
Ta	0.004	—	< 0.04		< 0.02		< 0.02		< 0.03		< 0.07		< 0.02	
Th	< 0.01		0.015	—	< 0.02		< 0.01		< 0.02		< 0.04		< 0.02	
U	< 0.01		< 0.03		< 0.01		< 0.01		< 0.02		0.023	0.005	0.029	0.007
Eu/Eu*	1.02		1.00		1.15		0.96		0.81		0.94		1.05	

[a] Concentrations are given in ppm (μg/g). ND = not determined. Cs, Ba, and Pb were measured but were below the detection limit in all samples analyzed. Typical detection limits are 0.2 ppm for Cs, 0.1 ppm for Ba, and 0.2 ppm for Pb.
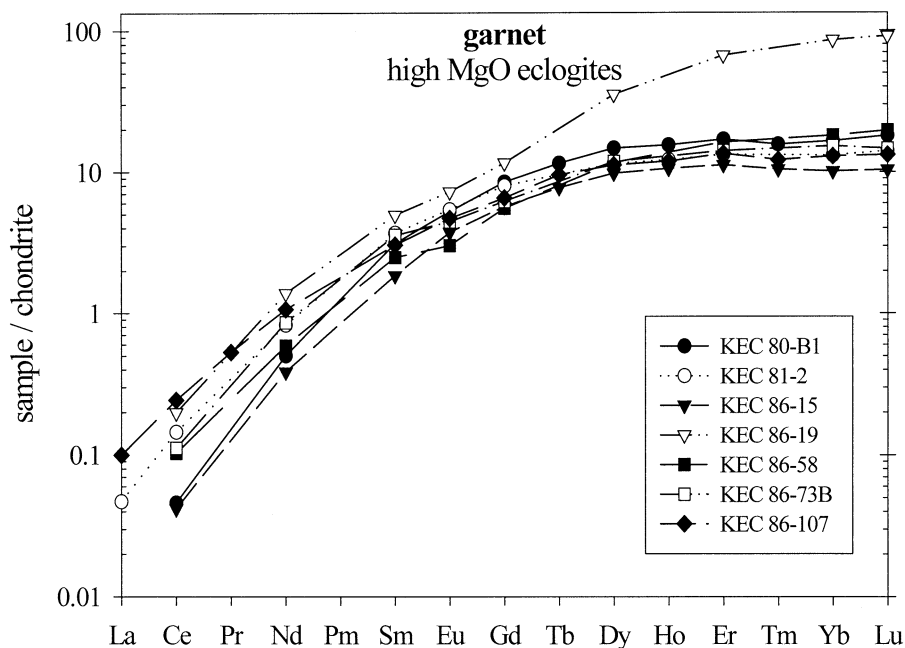

Fig. 2. Chondrite-normalized garnet REE data for Koidu high MgO eclogite xenoliths. Element abundances are normalized to the chondrite values of Boynton (1984).
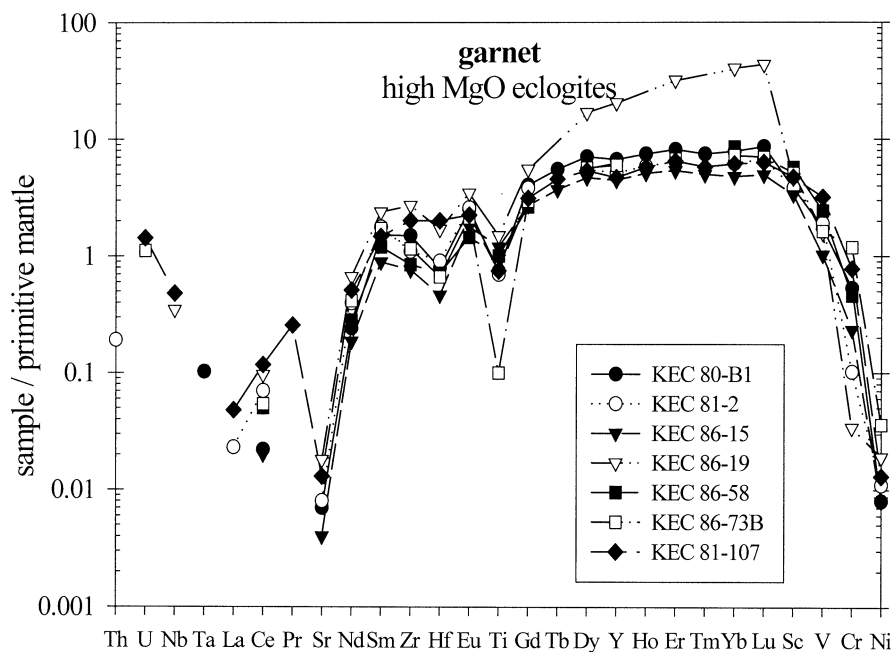
Fig. 3. Mantle-normalized garnet trace element diagram for Koidu high MgO eclogite xenoliths. Element abundances are normalized to the primitive mantle values of McDonough and Sun (1995).

negative Eu anomalies (Eu/Eu* = 0.89 and 0.87, respectively); no clinopyroxenes were observed to have positive Eu anomalies. The high MgO clinopyroxenes are significantly more LREE-enriched compared with clinopyroxenes of the low MgO eclogites (Barth et al., 2001). All clinopyroxenes show pronounced HFSE anomalies (Fig. 5). The concentrations of Rb and Cs are generally below the detection limit, whereas very small concentrations of Ba (0.1 to 0.6 ppm) have been measured.

Ilmenites (Table 4) have highly variable concentrations of Nb and Ta, with Nb/Ta ranging from subchondritic to superchondritic. The ilmenites have relatively homogeneous concentrations of W, Zr, Hf, V, and Ni. Ilmenites in the high MgO eclogites have trace element patterns similar to that of rutiles in the low MgO eclogites but have higher Ni and lower Zr and Hf concentrations.

4.3. Whole-Rock Chemistry

Trace element compositions of nine Koidu high MgO eclogite whole-rock powders were determined by solution ICP-MS (Table 5, Fig. 6) to assess the amount of trace element enrichment produced by secondary phases. All samples show variable enrichments in incompatible trace elements and relatively flat HREE patterns (except KEC 86-19, which is HREE enriched). Most samples have pronounced positive Nb anomalies and low Ti concentrations relative to REE. Some samples show negative Zr and Hf anomalies (e.g., KEC 86-58).

To evaluate the chemical composition of the eclogites before their entrainment in and interaction with the kimberlite, primary whole-rock compositions have been reconstructed on the basis of the trace element contents measured in primary garnet, clinopyroxene, and ilmenite by means of previously published modal abundances (Table 6; Hills and Haggerty, 1989; Fung and Haggerty, 1995).

Some trace elements, such as the HFSE, may be largely contained in accessory phases such as ilmenite. This presents a problem for whole-rock reconstructions, as it is generally difficult to determine precise modal proportions of accessory phases by point-counting such coarse-grained rocks. For this reason, we have calculated the modal abundance of ilmenite from Ti mass balance between the measured whole-rock and mineral compositions (see Rudnick et al., 2000, and Barth et al., 2001, for details). For the one sample lacking bulk rock TiO_2 concentrations (KEC 80-B1), modal ilmenite was calculated assuming that the bulk rock has no Ti-anomaly on a multi-element mantle-normalized diagram (Fig. 7).

The reconstructed high MgO eclogites have slightly LREE-depleted to LREE-enriched patterns with flat HREE, except KEC 86-19, which shows HREE-enrichment (Fig. 7). Two samples (KEC 86-58 and KEC 86-107) have negative Eu anomalies (Eu/Eu* = 0.83). These anomalies, however, might be caused by LREE enrichment rather than Eu depletion (see below). The reconstructed whole rocks show a wide range of Nb/La and Nb/Ta ratios, ranging from subchondritic to superchondritic (Fig. 7). The high MgO eclogites have low Zr concentrations relative to Sm. This Zr depletion is not due to overlooked accessory phases such as zircon in the whole-rock reconstructions because the measured whole rocks also show Zr depletions and zircon has not been observed, despite extensive searching for it. Note that the sample with the lowest HREE contents (KEC 86-15) has a positive Sr anomaly, whereas samples with higher HREE contents (e.g., KEC 86-107) have negative Sr anomalies. The eclogites have low to moderate U and Th contents with variable Th/U ratios.

Compared with the reconstructed whole rocks, measured whole rocks of these kimberlite-borne eclogite xenoliths are

Table 3. Trace element composition of clinopyroxene determined by LA-ICP-MS.[a]

Sample spots	KEC 80-B1		KEC 81-2		KEC 86-15		KEC 86-19		KEC 86-58		KEC 86-73B		KEC 86-107	
	n = 10	1σ	n = 9	1σ	n = 7	1σ	n = 7	1σ	n = 7	1σ	n = 2	1σ	n = 7	1σ
Sc	27.3	1.3	24.4	1.0	21.6	0.3	30.8	0.4	36.1	3.0	33.5	2.6	18.5	0.5
V	421	16	472	6	399	20	299	30	510	12	461	9	449	34
Cr	685	61	196	4	323	23	1232	430	740	42	2201	123	838	160
Ni	268	25	354	4	267	16	278	32	146	7	188	9	195	18
Ga	ND		ND		ND		ND		8.53	0.68	ND		ND	
Rb	< 0.1		< 0.4		< 0.1		< 0.2		< 0.8		< 0.3		< 0.08	
Sr	164	9	151	13	163	3	206	5	456	106	298	2	634	106
Y	4.18	0.12	2.51	0.20	2.03	0.09	4.07	0.09	5.32	0.64	5.25	0.12	1.80	0.08
Zr	45.5	1.5	21.2	1.9	27.9	0.5	43.8	2.6	14.0	1.3	32.3	1.1	19.5	1.4
Nb	0.16	0.04	< 0.3		< 0.04		0.29	0.04	< 0.6		0.73	0.03	1.75	0.13
Ba	0.13	0.03	0.40	0.05	0.12	0.02	0.21	0.01	0.54	0.19	0.32	0.02	0.58	0.12
La	5.04	0.32	8.35	1.18	1.88	0.11	3.40	0.10	24.75	7.76	14.87	0.69	16.89	1.52
Ce	14.6	0.7	24.5	3.0	6.57	0.29	13.5	0.4	57.3	13.5	43.2	2.0	69.91	6.89
Pr	2.27	0.06	ND		1.17	0.05	ND		ND		ND		11.57	1.51
Nd	12.2	0.4	15.4	1.1	6.29	0.21	12.5	0.2	21.8	2.9	27.8	1.8	47.34	5.73
Sm	3.57	0.22	3.52	0.28	1.80	0.04	3.25	0.10	2.84	0.23	4.68	0.31	4.98	0.79
Eu	1.08	0.05	0.90	0.09	0.58	0.04	0.93	0.03	0.72	0.02	1.30	0.00	0.84	0.10
Gd	3.16	0.14	2.15	0.18	1.53	0.09	2.57	0.09	2.16	0.07	3.67	0.18	1.74	0.06
Tb	0.35	0.01	ND		0.17	0.01	ND		ND		ND		0.16	0.01
Dy	1.52	0.10	0.94	0.12	0.77	0.03	1.36	0.06	1.43	0.10	1.72	0.10	0.66	0.05
Ho	0.19	0.01	0.11	0.02	0.09	0.01	ND		ND		ND		0.076	0.005
Er	0.34	0.03	0.19	0.02	0.16	0.02	0.36	0.02	0.45	0.08	0.39	0.02	0.16	0.01
Tm	0.026	0.004	ND		0.013	0.002	ND		ND		ND		0.015	0.002
Yb	0.11	0.01	0.082	0.012	0.067	0.005	0.17	0.02	0.24	0.04	0.18	0.04	0.067	0.010
Lu	0.012	0.003	0.003	—	0.005	—	0.019	0.002	0.030	0.008	0.024	0.001	0.007	0.002
Hf	2.24	0.11	1.23	0.16	1.55	0.06	3.22	0.17	0.68	0.05	1.19	0.06	1.50	0.13
Ta	0.007	0.002	< 0.02		0.006	0.003	0.030	0.008	< 0.02		0.063	0.006	0.11	0.04
Pb	ND		ND		ND		0.28	0.02	3.79	0.63	1.68	0.00	ND	
Th	0.44	0.06	0.46	0.08	0.069	0.018	0.039	0.005	1.07	0.25	0.51	0.04	0.26	0.05
U	0.11	0.02	0.069	0.013	0.015	0.003	0.012	0.002	0.16	0.03	0.11	0.01	0.067	0.011
Eu/Eu*	0.98		1.00		1.07		0.99		0.89		0.96		0.87	

[a] Concentrations are given in ppm (μg/g). ND = not determined. Cs was measured but below the detection limit (0.2 ppm) in all samples analyzed.

enriched in incompatible trace elements relative to the compositions reconstructed from the primary minerals (Fig. 8). Highly incompatible elements are affected more than moderately incompatible and compatible elements; for example, Ba shows extreme enrichment in the whole rock as a result of Ba contained on grain boundaries and in secondary phases

Table 4. Trace element composition of ilmenite determined by LA-ICP-MS.

Sample spots	KEC 80-B1		KEC 81-2		KEC 86-15		KEC 86-58		KEC 86-73B		KEC 86-107	
	n = 4	1σ	n = 8	1σ	n = 9	1σ	n = 1	1σ	n = 4	1σ	n = 4	1σ
Sc	7.5	0.9	7.2	1.4	4.8		13	—	10	1.7	17	5.1
V	1242	46	1378	44	1020	223	726	—	1008	23	2231	405
Cr	1191	28	654	74	637	131	797	—	3310	105	10554	3273
MnO wt%	0.25	0.04	0.20	0.03	0.22	0.06	0.46	—	0.31	0.01	0.42	0.04
Ni	1177	137	1977	118	1321	129	1550	—	945	81	1136	131
Zn	ND		ND		ND		76	—	114	4	221	48
Zr	111	4	95	3.5	41	15	34	—	134	9	846	209
Nb	64	0.4	1961	49	118	16	368	—	5740	42	4927	434
Mo	ND		ND		ND		< 4.5		< 1.5		2.0	0.43
Sn	ND		ND		ND		1.98	—	4.13	—	13.3	4.3
Sb	ND		ND		ND		< 0.4	—	< 1		< 2	
Hf	2.39	0.26	2.17	0.12	1.07	0.08	0.74	—	1.73	0.40	24.1	7.0
Ta	3.27	0.05	78.4	5.8	5.10	0.84	5.47	—	380	15	465	27
W	ND		ND		ND		1.48	—	0.80	0.14	0.48	0.27
Pb	ND		ND		< 0.2		0.33	—	< 0.9		< 2	
Th	0.021	0.024	0.005	0.004	< 0.02		0.22	—	< 0.1		0.027	0.024
U	0.17	0.07	0.15	0.15	0.05	0.05	0.32	—	0.079	0.034	0.25	0.22

[a] Concentrations are given in ppm (μg/g). ND = not determined. Ba, Rb, Sr, Y, and REE were measured but below the detection limit in all samples analyzed. Typical detection limits are 0.1 ppm for Ba, 0.5 ppm for Rb and Sr, and 0.3 ppm for REE.
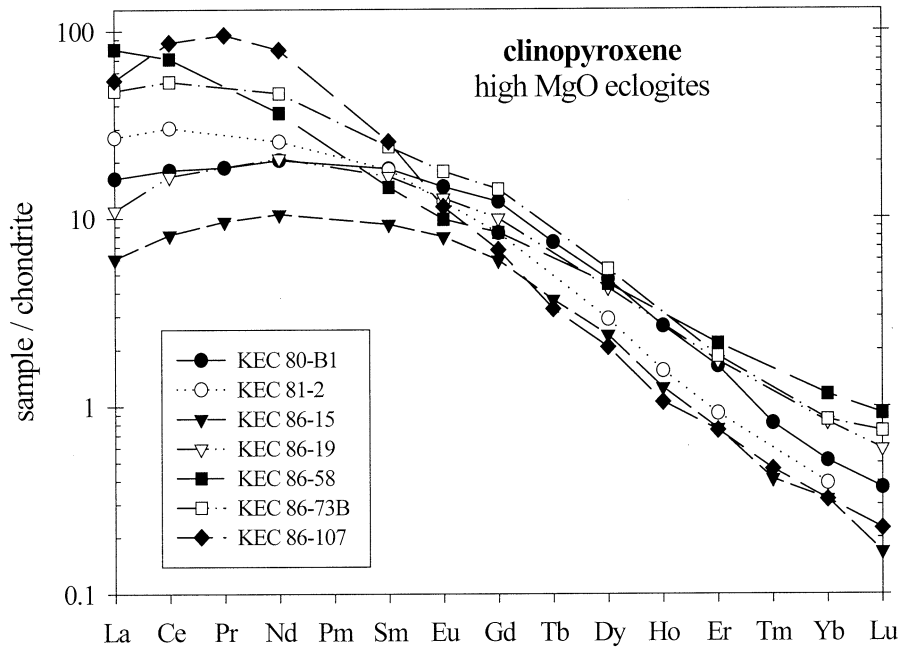
Fig. 4. Chondrite-normalized clinopyroxene REE data for Koidu high MgO eclogite xenoliths. Normalized as in Figure 2.

(e.g., phlogopite); La shows high and variable enrichments in the analyzed whole rock compared with the reconstructed rock, whereas Yb and Y are little affected by alteration. Except for ilmenite, accessory phases (e.g., apatite, zircon) can be ruled out as important hosts of trace elements because these phases are not observed in the samples.

5. METASOMATIC OVERPRINTING

5.1. Modal Metasomatism

Enrichment of incompatible trace elements caused by infiltration and alteration by the host kimberlite, or fluids derived therefrom, is manifested by the presence of secondary phlogo-
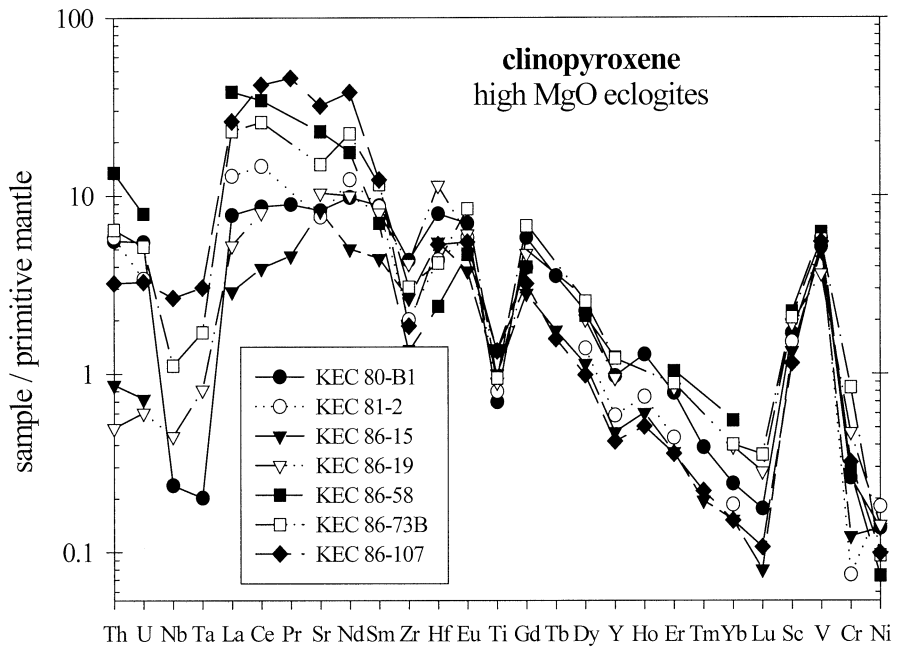
Fig. 5. Mantle-normalized clinopyroxene trace element diagram for Koidu high MgO eclogite xenoliths. Normalized as in Figure 3.

Table 5. Whole rock compositions of the Koidu high MgO eclogites measured by solution ICP-MS; concentrations are given in ppm (μg/g).

Element	KEC-81-2	KEC 81-AB-11	KEC 86-15	KEC 86-19	KEC 86-58	KEC 86-73A	KEC 86-73B	KEC 86-90	KEC 86-107
Ga	10.5	9.08	10.6	10.7	8.76	10.1	7.95	10.8	8.55
Rb	14.3	2.83	11.0	13.7	3.30	7.01	11.0	7.49	7.91
Sr	244	369	119	112	218	101	316	44.3	85.2
Y	17.7	27.7	16.7	47.3	20.7	25.6	21.9	16.4	15.8
Zr	39.9	93.6	33.8	73.4	19.2	38.0	39.9	23.1	34.6
Nb	50.0	44.7	13.5	13.1	12.6	11.4	41.1	9.52	25.9
Cs	0.14	0.05	0.19	0.13	0.07	0.11	0.24	0.25	0.47
Ba	349	214	257	193	162	198	622	68.9	115
La	27.4	26.7	7.71	6.28	16.7	7.85	16.3	3.47	5.08
Ce	55.2	68.6	15.6	16.3	37.6	17.2	43.2	7.47	14.1
Pr	6.33	8.60	1.86	2.43	4.33	2.18	6.17	0.93	2.10
Nd	23.6	33.2	7.10	10.7	14.6	8.86	24.5	3.84	9.34
Sm	4.07	5.72	1.58	2.53	2.23	2.33	4.38	1.19	2.30
Eu	1.20	1.65	0.65	0.91	0.63	0.80	1.38	0.48	0.72
Gd	3.85	5.19	2.07	3.34	1.68	3.06	3.77	1.97	2.24
Tb	0.57	0.78	0.39	0.73	0.42	0.55	0.60	0.37	0.36
Dy	3.28	4.75	2.48	5.65	3.04	3.79	3.59	2.54	2.34
Ho	0.69	1.02	0.58	1.64	0.74	0.89	0.74	0.60	0.55
Er	1.98	3.02	1.78	5.86	2.40	2.72	2.14	1.56	1.63
Yb	1.94	3.01	1.54	6.95	2.43	2.80	1.95	1.29	1.46
Lu	0.30	0.47	0.23	1.10	0.37	0.46	0.30	0.17	0.23
Hf	1.09	2.44	0.87	2.26	0.51	1.13	0.92	0.53	0.70
Th	2.04	1.41	0.92	1.03	1.53	0.89	1.51	0.54	0.74
U	0.44	0.34	0.23	0.28	0.33	0.32	0.34	0.13	0.27

pite, amphibole and other phases (e.g., carbonates, sulfides, spinel) in veins and on grain boundaries. These phases may constitute up to 20 modal percent of the minerals in some xenoliths (Hills and Haggerty, 1989). This kimberlite-related "modal metasomatism" is pervasive in both low MgO and high MgO eclogites and has dramatic consequences for whole rock incompatible element chemistry (Fig. 8; also fig. 8 in Barth et al., 2001) and even whole-rock MgO contents (Fung and Haggerty, 1995). In some high MgO eclogites, primary clinopyroxene, which is depleted in Rb, Ba, Nb, and Ta, is partially replaced by secondary amphibole that has much higher concentrations of these elements (Fig. 9). However, the secondary amphibole has similar concentrations of the other incompatible trace elements to the primary clinopyroxene, suggesting that the amphibole inherited these elements from the clinopyroxene. This observation demonstrates that amphibole is not in high-temperature trace element equilibrium with clinopyroxene, and indicates that the secondary amphibole grew shortly before the eruption of the host kimberlite (see below).

5.2. Cryptic Metasomatism

Cryptic metasomatism is defined as enrichment of incompatible elements such as Rb, Sr, Ba, and REE without visible evidence of metasomatism (Dawson, 1984). This style of metasomatism, which was not observed in the Koidu low MgO eclogites, can occur, in addition to modal metasomatism, in the Koidu high MgO eclogites. In some Koidu high MgO eclogites (KEC 86-15, KEC 86-19, and KEC 86-107), analyses of optically unaltered, crack-free minerals reveal trace element concentrations that are significantly higher than in other grains of the same mineral, which are both optically and chemically indistinguishable (Barth, 2001). For example, in sample KEC 86-15, one phase of garnet is depleted in LREE and other

highly incompatible elements, whereas the other garnet contains noticeable concentrations of these elements (Fig. 10). As garnet in trace element equilibrium with clinopyroxene and ilmenite is expected to contain low concentrations of Sr and LREE, which partition into clinopyroxene (Harte and Kirkley, 1997), and Nb and Ta, which partition into ilmenite, the first garnet is considered to be primary. The high concentrations of Sr and LREE in the altered garnet preclude equilibrium with the other primary phases in the eclogite. This type of metasomatism, where major element and incompatible trace element concentrations are decoupled and concentrations of trace elements such as Sr apparently disobey normal partitioning relationships, has been named isolated trace element enrichment by Harte (1987).

5.3. Origin of Metasomatic Component

5.3.1. Host kimberlite

Both the modal and cryptic metasomatism described above are most likely related to infiltration or exchange with a kimberlitic magma (or a fluid derived therefrom) because Ba, Sr, Nb, Ta, and LREE are highly enriched in kimberlites compared with the primary eclogite minerals (Figs. 9 and 10). Trace element data suggest that the liquids giving rise to the metasomatism, although not necessarily identical to the kimberlite carrying the xenoliths to the surface, have probably formed part of the same set of magmatic events (cf. Harte, 1987). Thus, the trace element pattern of the altered garnet in KEC 86-15 is approximately parallel to that of the host kimberlite for the most incompatible elements (Fig. 10).

These metasomatic enrichments must have occurred shortly before the eruption of the host kimberlite because at the high equilibration temperatures these eclogites experienced (1080 to 1130°C), diffusion would rapidly erase such fine-scale trace
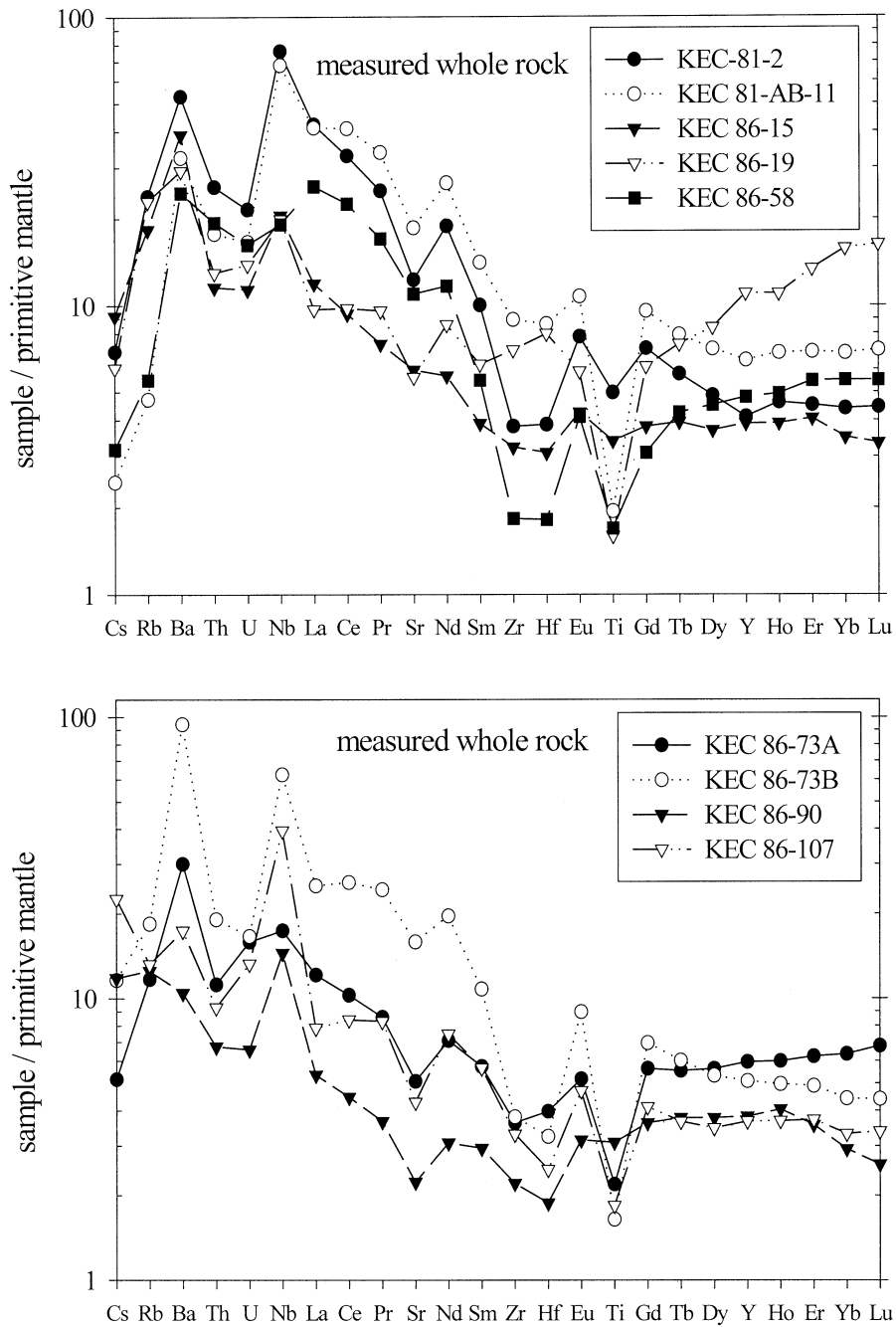
Fig. 6. Mantle-normalized measured whole-rock trace element diagrams for Koidu high MgO eclogite xenoliths. Samples are sorted by number. Normalized as in Figure 3.

element disequilibrium. The experimentally determined diffusion coefficient of Sr in garnet at the equilibration temperature of KEC 86-15 (1100°C) is 1.6% 10^{-16} cm^2/s (Coghlan, 1990). Thus, taking $t = (d^2/4D)$ as the homogenization time (t) for a sphere (diameter d) with diffusion coefficient D, we calculate that a grain 4 mm in diameter would be homogenized in ~8 Ma.

5.3.2. Ancient metasomatism

Although its likely that most of the modal and cryptic metasomatic features described above relate to recent kimberlite-

eclogite interaction, several features of the eclogite compositions suggest that they may have also experienced more ancient metasomatism. Metasomatism by passing melts, before the kimberlite-related alteration, can lead to increased Mg# (molar Mg/(Mg+Fe)), Ba, Nb, Zr, and LREE contents of the original eclogite (Dawson, 1984; Harte, 1987; Zindler and Jagoutz, 1988; Ireland et al., 1994). Some Koidu high MgO eclogites are LREE-enriched and have "humps" in their REE pattern (e.g., KEC 86-107, Fig. 11). Such REE patterns are predicted for early stages of metasomatism by melt percolation models

Table 6. Reconstructed whole rock compositions of the Koidu high MgO eclogites.[a]

Element	KEC 80-B1 1.6% ilm	KEC 81-2 1.7% ilm	KEC 86-15 0.92% ilm	KEC 86-19 no ilmenite	KEC 86-58 0.28% ilm	KEC 86-73B 0.46% ilm	KEC 86-107 0.36% ilm
	c	wr	wr	wr	wr	wr	wr
SiO_2	48.18	48.20	48.30		49.43	48.74	46.79
TiO_2	0.94	1.00	0.68		0.34	0.33	0.37
Al_2O_3	12.80	12.86	13.48		12.63	12.88	16.37
FeO	8.88	9.10	9.84		4.55	7.87	5.75
MnO	0.18	0.22	0.22		0.18	0.33	0.22
MgO	16.14	15.62	15.63		19.36	17.22	18.67
CaO	12.14	12.64	10.35		12.38	12.03	10.06
Na_2O	1.53	1.30	1.80		1.08	1.22	1.06
Total	100.10	100.13	100.06		100.00	100.63	99.45
Mg#	76.4	75.4	73.9		88.4	80.2	85.3
Sc	44	43	39	53	64	59	57
Ti	5633	5989	4072	1432	2035	1985	2212
V	300	332	239	216	356	294	330
Cr	1037	239	478	673	972	2683	1676
Ni	161	219	144	160	77	131	85
Sr	82	74	76	105	227	143	209
Y	16	12	11	45	16	16	14
Zr	32	18	18	36	11	22	24
Nb	1.1	34	1.1	0.3	1.0	27	19
La	2.5	4.1	0.9	1.7	12	7.1	5.6
Ce	7.3	12	3.1	7.0	29	21	23
Pr	1.1	ND	0.5	ND	ND	ND	3.8
Nd	6.3	7.8	3.1	6.8	11	14	16
Sm	2.1	2.1	1.0	2.1	1.7	2.6	2.0
Eu	0.7	0.6	0.4	0.7	0.5	0.8	0.5
Gd	2.6	2.1	1.5	2.8	1.8	2.6	1.7
Tb	0.4	ND	0.3	ND	ND	ND	0.4
Dy	3.1	2.3	2.0	6.2	2.6	2.8	2.6
Ho	0.6	0.5	0.4	ND	ND	ND	0.6
Er	1.9	1.5	1.3	7.0	1.9	1.7	1.9
Yb	1.7	1.4	1.1	8.8	2.0	1.7	1.8
Lu	0.29	0.22	0.18	1.4	0.33	0.26	0.29
Hf	1.3	0.77	0.80	1.9	0.44	0.67	0.96
Ta	0.058	1.3	0.060	0.015	0.015	1.8	1.7
Th	0.22	0.23	0.032	0.020	0.53	0.24	0.084
U	0.059	0.037	0.007	0.006	0.081	0.062	0.042
Eu/Eu*	0.94	0.94	1.03	0.93	0.83	0.93	0.83

[a] Major and trace element concentrations are given in wt% and ppm (μg/g), respectively. wr = modal amount of ilmenite calculated by mass balance using whole rock Ti contents. c = modal amount of ilmenite calculated assuming no Ti anomaly. See text for details. ND = not determined. For sample KEC 86-19, major element compositions could not be calculated because garnet and clinopyroxene are strongly zoned. Mineral modes and major element compositions are published in Hills and Haggerty (1989).

(Navon and Stolper, 1987). Furthermore, the high MgO eclogites have Mg#s (74 to 88) that overlap or exceed the Mg#s of the metasomatized eclogites of Ireland et al. (1994) (Mg# 74) and primitive, peridotite-derived melts (Mg# 74 to 80). In addition, primary (texturally equilibrated) amphibole in one Koidu sample (KEC 81-AB-11) has been cited as evidence for mantle metasomatism that predated the kimberlite-related metasomatism (Hills and Haggerty, 1989). Thus, in addition to the recent kimberlite-associated metasomatism documented above, we conclude that at least some of the high MgO eclogites have experienced ancient metasomatism that resulted in an enrichment of highly incompatible elements.

For this reason, we will focus our discussion of the petrogenesis of the high MgO eclogites on understanding the variations observed within the "conservative elements"—those such as the HREE and transition metals (cf. Figs. 9 and 10), which are less likely to have been influenced by metasomatic overprinting, recent or ancient. Some features of more incompatible element patterns may also be utilized, if these features can be demonstrated to be robust indicators of protolith composition.

6. ORIGINS OF THE KOIDU HIGH MGO ECLOGITES

The Koidu low MgO eclogites are interpreted to represent ancient altered oceanic crust that underwent an episode of partial melting during subduction (Rollinson, 1997; Barth et al., 2001). Weak correlations between MgO, Ni, and Cr (Fig. 12) and an apparent compositional gap between the two types of eclogites (Hills and Haggerty, 1989), suggest that the high MgO eclogites are not simply picritic equivalents of the low MgO eclogites (Hills and Haggerty, 1989) and that the two varieties are not related to each other by simple partial melting or crystal fractionation trends.

Although the high MgO eclogites have general chemical affinities to picrites (Fig. 14; Hills and Haggerty, 1989), this does not hold true in detail (Fig. 13). The high MgO eclogites
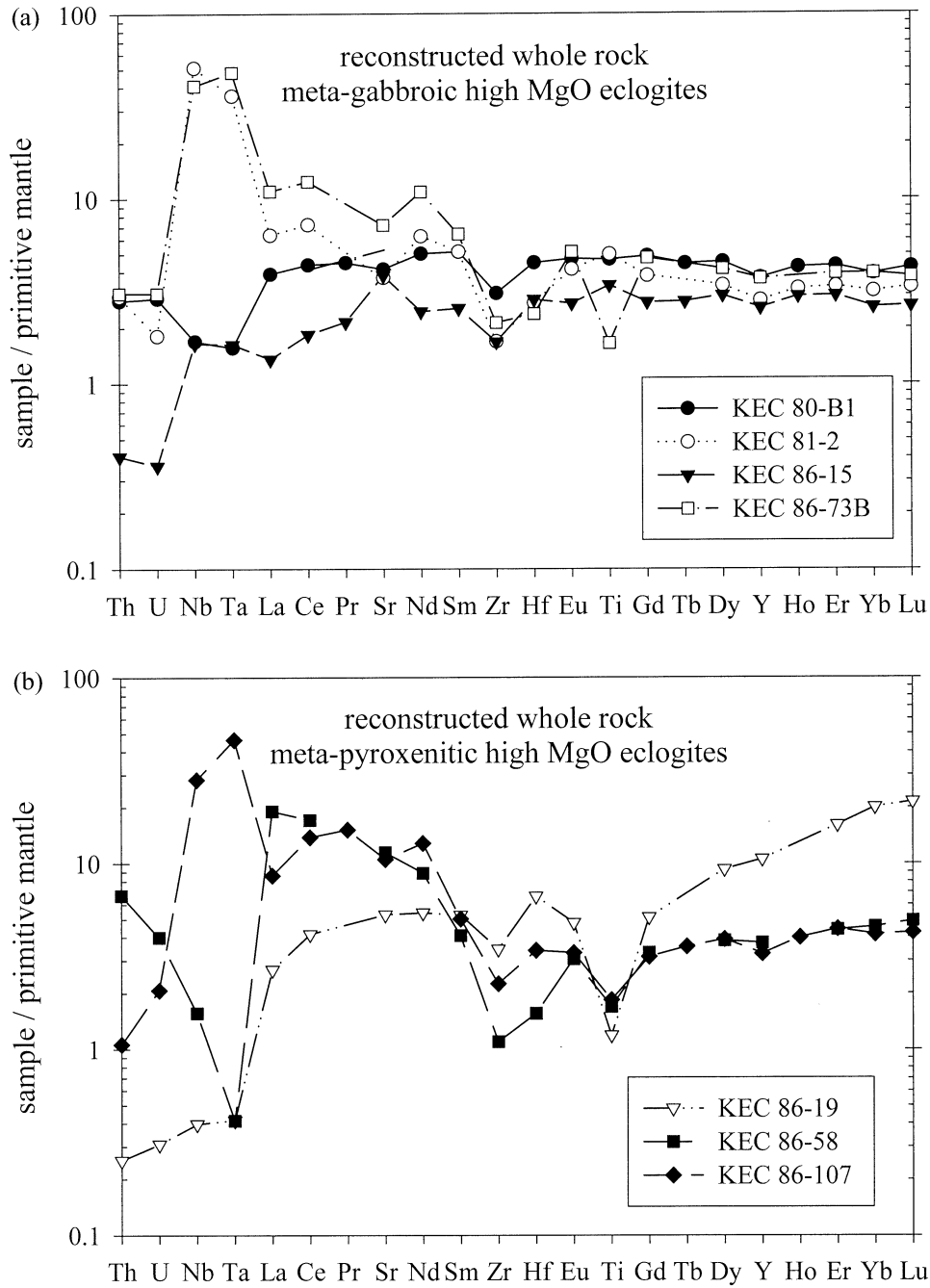
Fig. 7. Mantle-normalized reconstructed whole-rock trace element diagram for Koidu high MgO eclogite xenoliths. (a) High MgO eclogites interpreted as metagabbros. (b) High MgO eclogites interpreted as metapyroxenites See text for reconstruction procedure. Normalized as in Figure 3.

have higher Al_2O_3 and lower FeO contents than picrites (and higher Mg#s than Archean basalts). Moreover, eclogites that are both high in MgO and Al_2O_3 (e.g., KEC 86-107) do not represent reasonable liquid compositions. That is, the high MgO eclogites have, on average, higher Al_2O_3, slightly higher Na_2O, lower FeO, and slightly lower MgO contents than primary high-pressure (4 GPa) picritic mantle melts (Figs. 13 and 14). At the same time, several samples are more MgO-rich than experimental low-pressure (1 GPa) peridotite melts (Figs. 13

and 14). The high Mg#s (74 to 88) of the high MgO eclogites point toward an origin as cumulates.

Major element geochemistry does not allow us to distinguish between a low-pressure and high-pressure cumulate origin for these eclogites; the compositions of the Koidu high MgO eclogites overlap with the highly variable compositions of both gabbros and with pyroxenites (Figs. 13 and 14). The presence of accessory silica phases such as coesite or quartz pseudomorphs after coesite in other high MgO eclogites has been
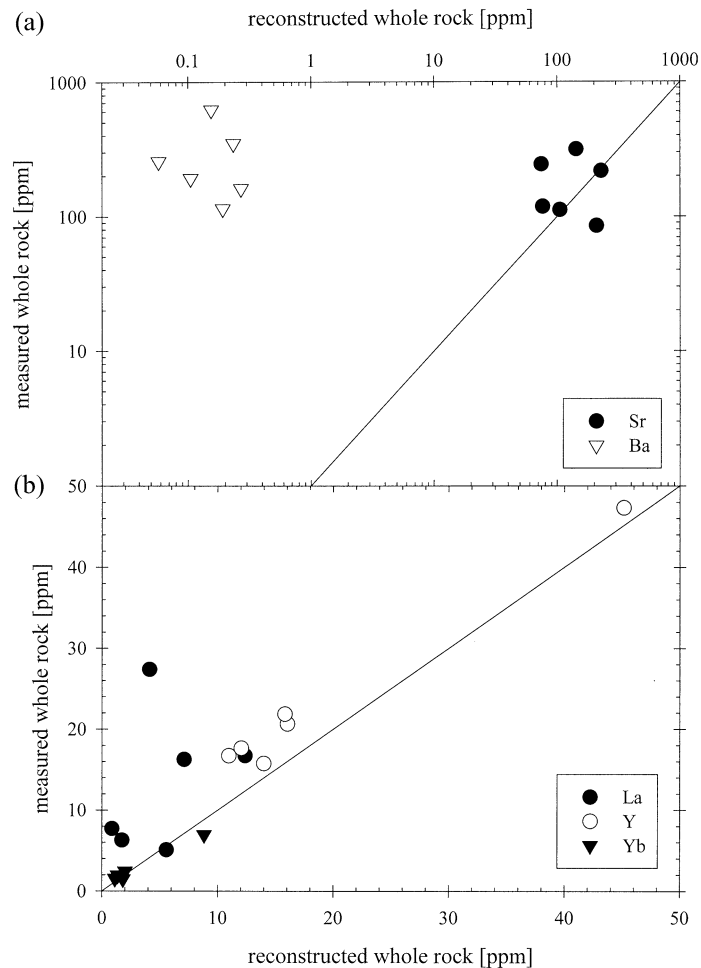
Fig. 8. Plot of the reconstructed whole-rock compositions vs. the measured whole-rock compositions for selected elements from the Koidu high MgO eclogites. (a) Sr (solid circles) and Ba (open upside-down triangles). Eclogite KEC 86-107 has lower Sr in the measured whole rock than in the recalculated whole rock, probably because of sample heterogeneity. (b) La (solid circles), Y (open circles), and Yb (solid upside-down triangles).

suggested to rule out a high-pressure mantle origin for these rocks (e.g., Schulze and Helmstaedt, 1988). Although coesite is common in some suites of eclogites with basaltic bulk composition (e.g., Roberts Victor eclogites, Schulze et al., 2000) and occurs in one of the low MgO suite eclogites from Koidu (Hills and Haggerty, 1989), it is generally rare in very magnesian eclogites (Zhang et al., 1996; Schulze et al., 2000) and has not been observed in the Koidu high MgO suite (Hills and Haggerty, 1989; Fung and Haggerty, 1995). Therefore, we turn to trace element modeling to test the cumulate origin for the Koidu high MgO eclogites and to see if any constraints can be placed on their original depth of formation.

REE and Sr contents are calculated for melts derived from low-pressure partial fusion of spinel peridotite and high-pressure partial fusion of garnet peridotite, as well as for cumulates (with or without trapped melt) that precipitate from such melts (model parameters are given in the figure caption of Fig. 11). REE and Sr patterns suggest low-pressure accumulation of olivine and plagioclase for some samples and high-pressure

accumulation of garnet and clinopyroxene for the rest of the samples (Fig. 11).

6.1. Low-Pressure Origin as Cumulate Gabbro and Layered Intrusions

Several samples (KEC 80-B1, KEC 81-2, KEC 86-15, and KEC 86-73B) have flat middle to heavy REE patterns, which suggests that garnet did not play a significant role during mantle melting and crystal accumulation. The eclogite with the lowest HREE content (KEC 86-15) has a positive Sr anomaly, which may be indicative of low-pressure plagioclase fractionation (Fig. 11). Although plagioclase has a positive Eu anomaly, the absolute REE concentrations in plagioclase are low and clinopyroxene dominates the REE budget of the cumulate. In contrast, plagioclase has high Sr contents and imposes a positive Sr anomaly on the cumulate. Mixing of a 15% nonmodal batch melt of depleted MORB-type spinel lherzolite with an ol-plag-opx-cpx cumulate in equilibrium with such a melt can reproduce the observed eclogite compositions if the cumulate
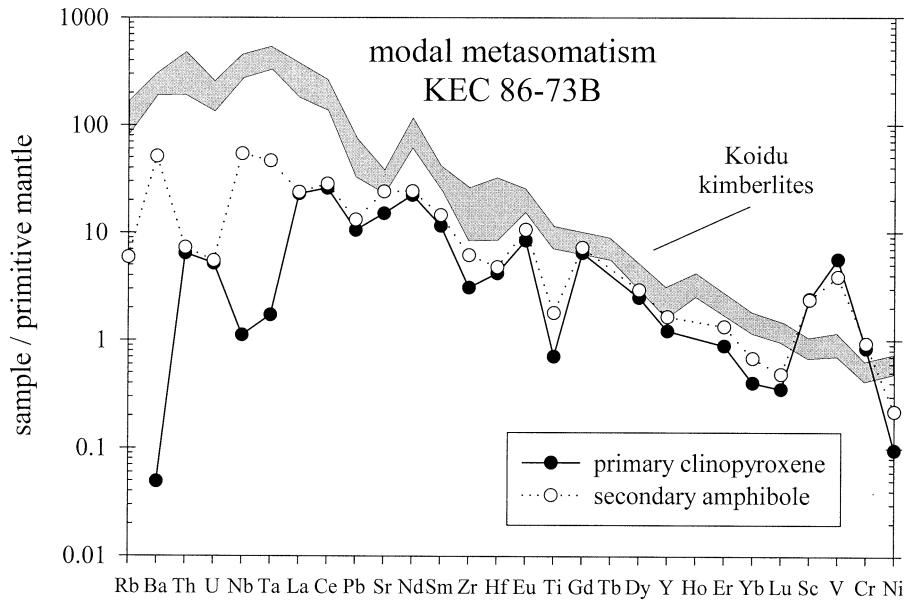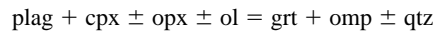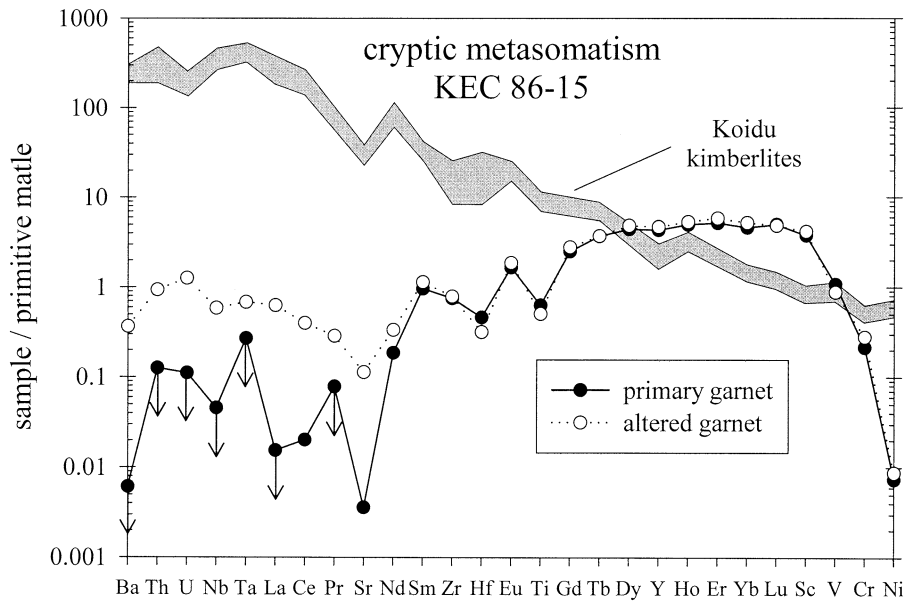
Fig. 9. Mantle-normalized trace element diagram illustrating kimberlite-related modal metasomatism of clinopyroxene in high MgO eclogite KEC 86-73B. Gray field shows the range of kimberlite compositions at Koidu, Sierra Leone (Taylor et al., 1994). Solid circles = the primary clinopyroxene composition; open circles = secondary amphibole replacing clinopyroxene. Normalized as in Figure 3.

portion is allowed to vary between 0 to ~33% (Fig. 11). Considering the evidence for metasomatic overprinting and the uncertainties in the parameters involved, the correspondence between the observed and calculated eclogite compositions is good.

CIPW norms (Hills and Haggerty, 1989) are consistent with olivine gabbros as precursors of the high MgO eclogites. On average, the high MgO eclogites contain 40% normative pla-

gioclase, 14% clinopyroxene, 12% opx, and 29% olivine. Note that olivine breaks down during eclogite-facies metamorphism by reactions of the type

$$plag + cpx \pm opx \pm ol = grt + omp \pm qtz$$

(e.g., Green and Ringwood, 1967; Mottana et al., 1990).

Fig. 10. Mantle-normalized trace element diagram illustrating kimberlite-related cryptic metasomatism of garnet in high MgO eclogite KEC 86-15. Gray field shows the range of kimberlite compositions at Koidu, Sierra Leone (Taylor et al., 1994). Solid circles = the primary garnet composition; open circles = garnet affected by cryptic metasomatism; arrows = elemental concentrations below the detection limit. Normalized as in Figure 3.
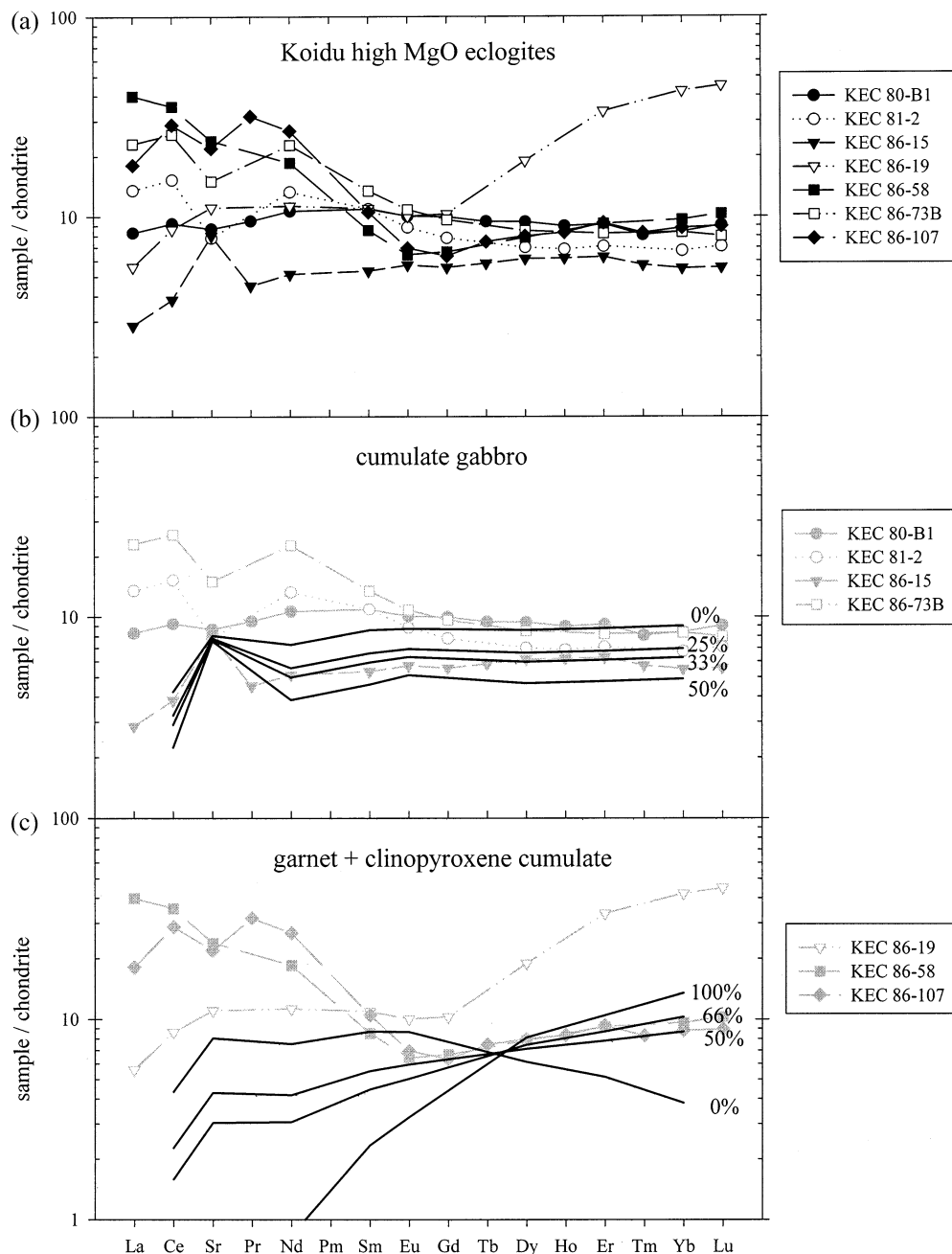
Fig. 11. Chondrite-normalized trace element diagram for the Koidu high MgO eclogite xenoliths. (a) Reconstructed whole-rock composition. (b) High MgO eclogites interpreted to be gabbroic low-pressure cumulates are shown in grey. Black lines are calculated compositions of a 15% nonmodal batch melt of depleted MORB-type spinel lherzolite with variable amounts of an ol-plag-opx-cpx cumulate in equilibrium with such a melt. The cumulate consists of 40% plagioclase, 30% olivine, 15% clinopyroxene, and 15% orthopyroxene, comparable to the CIPW norms of the high MgO eclogites. Numbers give the percentage of cumulate added. (c) High MgO eclogites interpreted to be pyroxenitic high-pressure cumulates are shown in gray. Black lines are calculated compositions of a 15% nonmodal batch melt of depleted MORB-type garnet lherzolite with variable amounts of a garnet–clinopyroxene cumulate in equilibrium with such a melt. Garnet and clinopyroxene crystallize in equal amounts. Numbers give the percentage of cumulate added. Initial composition, source mineralogy, melting phase proportions, and partition coefficients were taken from Johnson et al. (1990), Johnson and Dick (1992), Kelemen et al. (1993), Blundy and Wood (1994), Johnson (1998), and Bizimis et al. (2000). Normalized as in Figure 2.

Typical oceanic gabbros have relatively evolved compositions, close to those of basaltic melts, because the cotectic proportions of olivine, plagioclase, and pyroxene have a basal-tic bulk composition (cf. Dick et al., 2000). In this respect, such gabbros are more similar to the Koidu low MgO eclogites than to the high MgO eclogites. For example, the average oceanic
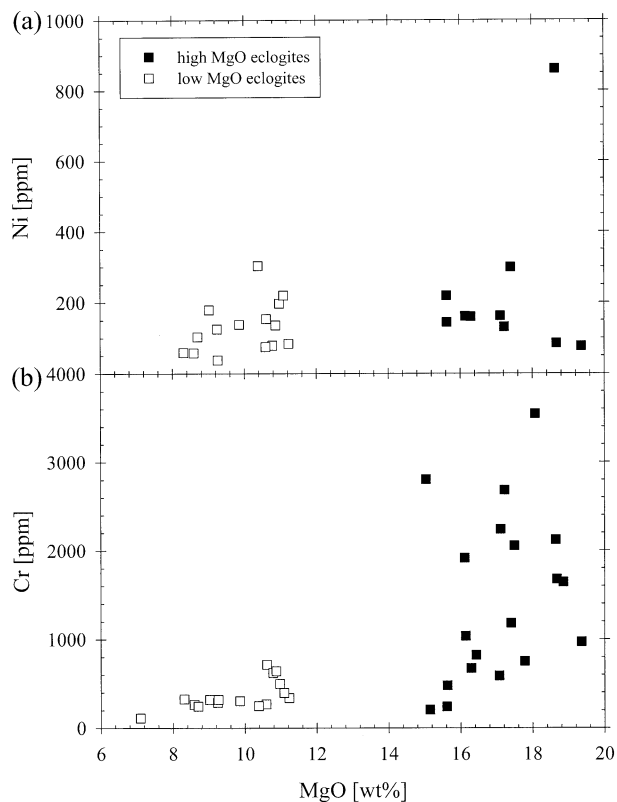
Fig. 12. Plot of reconstructed whole-rock MgO vs. Ni (a) and Cr (b). Solid squares = Koidu high MgO eclogite xenoliths (this study); open squares = Koidu low MgO eclogites (Barth et al., 2001).

gabbro of Hart et al. (1999) has 8.8 wt% MgO and Mg# = 62.9 (cf. 9.7 wt% MgO and Mg# = 59.5 for average low MgO eclogite and 17.1 wt% MgO and Mg# = 80.4 for average high MgO eclogite). However, olivine gabbros and troctolites, which can be found in the deeper, more mafic parts of gabbroic cumulates in oceanic crust, ophiolites, and layered intrusion, have whole-rock compositions with high MgO and Al_2O_3 contents similar to the high MgO eclogites. For instance, gabbros and troctolites recovered from DSDP Site 334 (Aumento et al., 1977) show increasing MgO content (from 10 to 22 wt%) with depth (Gunn and Roobol, 1977). The inferred crystallization sequence of the Site 334 gabbro suite is olivine followed by plagioclase, clinopyroxene, and finally orthopyroxene or pigeonite (Hodges and Papike, 1976), similar to the 1 bar normative mineralogy of the high MgO eclogites. The transition element contents of the high MgO eclogites are also consistent with an origin as olivine-pyroxene-plagioclase cumulates. Both the gabbros from DSDP Site 334 and the high MgO eclogites have comparatively low contents of Cr and Ni (Fig. 15).

6.2. In Situ Origin as Cumulates of Primary High-Pressure Melts

Three of the seven analyzed samples (KEC 86-19, KEC 86-58, and KEC 86-107) have fractionated HREE patterns (Fig. 11). Such HREE enrichments are rarely observed in the low MgO eclogites and probably reflect cumulate (or residual)

garnet. Mixing of a 15% nonmodal batch melt of depleted MORB-type garnet lherzolite with 50 to 66% of a garnet-cpx cumulate in equilibrium with such a melt can reproduce the observed HREE contents of two of these samples (KEC 86-58 and KEC 86-107; Fig. 11). KEC 86-107 has Yb contents about three times higher than the calculated garnet–clinopyroxene cumulate; such high concentrations cannot be accounted for with the model parameters chosen.

In support of the garnet–clinopyroxene cumulate hypothesis, the high MgO eclogites have major element compositions similar to pyroxenite xenoliths and pyroxenite veins in ophiolites (Figs. 13 and 14), which have been interpreted as cumulates of mafic magmas (e.g., Frey, 1980; Bodinier et al., 1987; Pearson et al., 1993). The high MgO eclogites have high Mg#s (74 to 88); some of them higher than primary high-pressure melts (Mg# = 76–80 at 4 GPa; Walter, 1998), moderate Cr and low Ni contents (Fig. 15) combined with low V contents, LREE-enriched clinopyroxene, and mantlelike $\delta^{18}O$ values. These features are broadly similar to the Group A eclogites from South Africa (Taylor and Neal, 1989), which have been interpreted as high-pressure cumulates of a basaltic melt. In this scenario, the LREE enriched whole-rock compositions are attributed to trapped liquid (Shervais et al., 1988; Taylor and Neal, 1989).

An observation that is difficult to reconcile with an origin of the Koidu high MgO eclogites as cumulates derived from primary mantle melts is the absence of modal olivine. As first pointed out by Hatton and Gurney (1987), volatile-free partial melting of peridotite at pressures exceeding ~3.5 GPa is not a feasible process for the generation of bimineralic eclogites, because olivine is one of the liquidus phases of such partial melts (cf. Hess, 1992). One way to circumvent this difficulty is to form the eclogite by fractional crystallization from a melt generated at pressures <3.3 GPa followed by reequilibration in the diamond stability field. Another possibility is to suppose that the source rock was itself olivine-free. In support of this possibility, some garnet pyroxenites and eclogites have been interpreted to represent high-pressure cumulates from silicic melts of subducted oceanic crust (Hatton and Gurney, 1987; Pearson et al., 1991). Because no unambiguous contact relationships between high MgO eclogite and ambient peridotitic mantle have been observed—that is, no composite xenoliths have been reported at Koidu, it remains unresolved if the Koidu high MgO eclogites are cumulates from a melt derived from an olivine-free source rock and crystallized at high pressures or if the high MgO eclogites were formed at lower pressures and reequilibrated in the diamond stability field.

6.3. Tectonic Setting of the Protoliths of the High MgO Eclogites

The Koidu high MgO eclogites can be subdivided into two types: metagabbroic cumulates and meta–garnet–pyroxenitic cumulates. This subdivision is similar to the type III eclogites occurring in ultramafic country rocks in the Dabieshan-Sulu region of China (Cong, 1996). The protoliths of some of these Mg-rich eclogites (type III-1) have been interpreted to be pyroxenitic cumulates derived from the continental mantle; others (type III-2) may have originated in a layered ultramafic-gabbro body of continental affinity (Zhang et al., 1994; Zhai
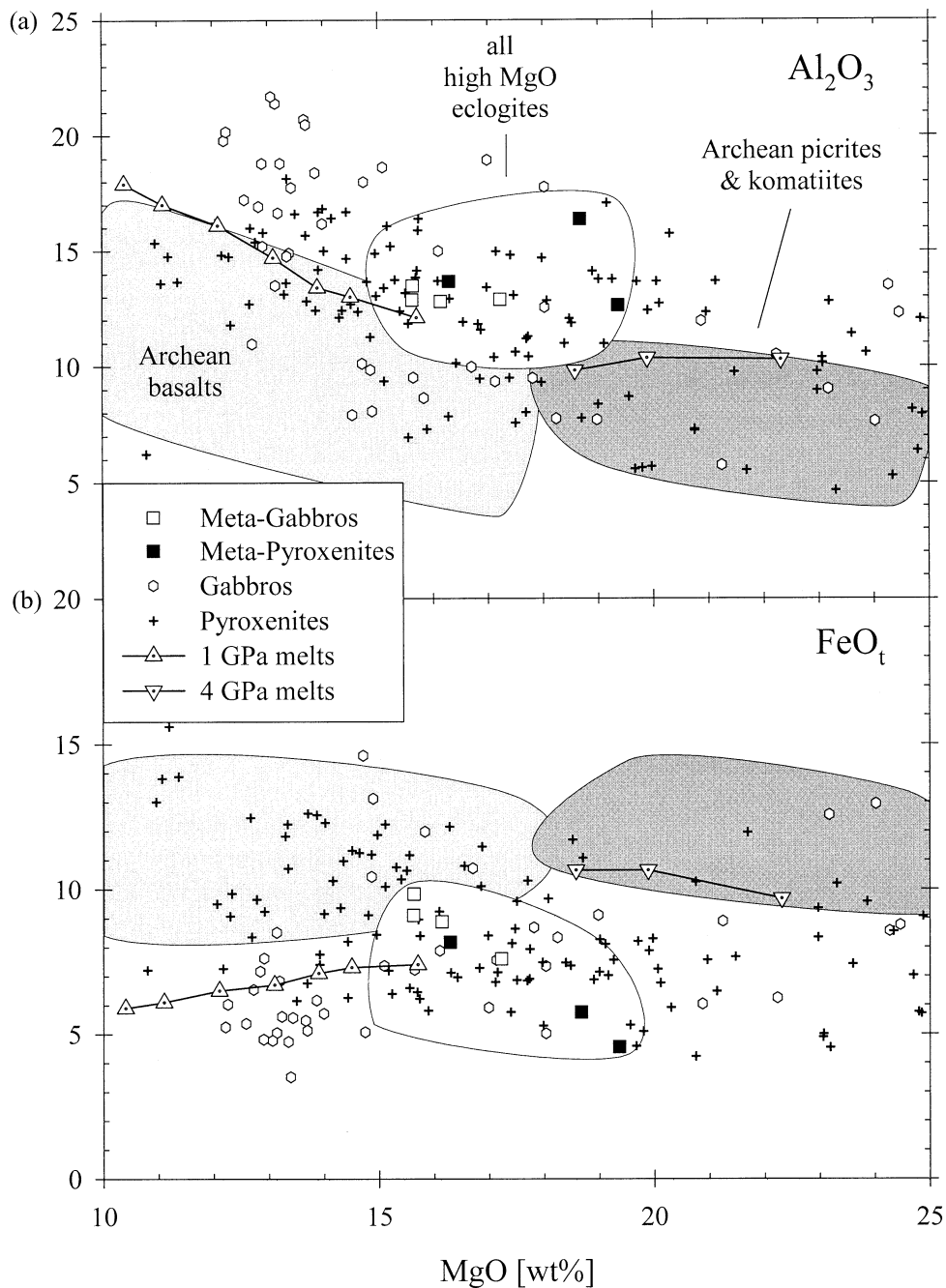
Fig. 13. Whole-rock MgO content plotted against Al_2O_3 (a) and total FeO (b) concentration. The white field shows the reconstructed whole-rock compositions of all the Koidu high MgO eclogites reported in Hills and Haggerty (1989) and Fung and Haggerty (1995). Pressure estimates of the high MgO eclogites cluster between 4.0 and 4.5 GPa. Open squares: high MgO eclogites interpreted here as metagabbros. Solid squares: high MgO eclogites interpreted as metapyroxenites. Crosses = Pyroxenite veins in ophiolites (Loubet and Allègre, 1982; Pearson et al., 1993) and pyroxenite xenoliths (Irving and Green, 1970; Wilkinson, 1975; Frey, 1980; Griffin et al., 1988; Kumar et al., 1996); dotted triangles and upside-down triangles = experimental pyrolite melts at 1 and 4 GPa, respectively (Baker and Stolper, 1994; Walter, 1998); open circles = oceanic gabbros (Gunn and Roobol, 1977; Dick et al., 1999; Hart et al., 1999). Light and dark gray fields show Archean basalts and Archean picrites and komatiites, respectively (compiled from the literature).

and Cong, 1996). Unlike the Dabieshan-Sulu eclogites, the Koidu eclogites do not show any indications of continental affinity.

The metagabbroic Koidu high MgO eclogites could represent deep cumulus portions of oceanic crust originally subducted to great depths. It remains unresolved if the high MgO eclogites experienced an episode of partial melting during subduction. Although the LREE-enriched patterns of some high MgO eclogites do not support partial melting, these incompatible elements have been variably reenriched by metasomatism
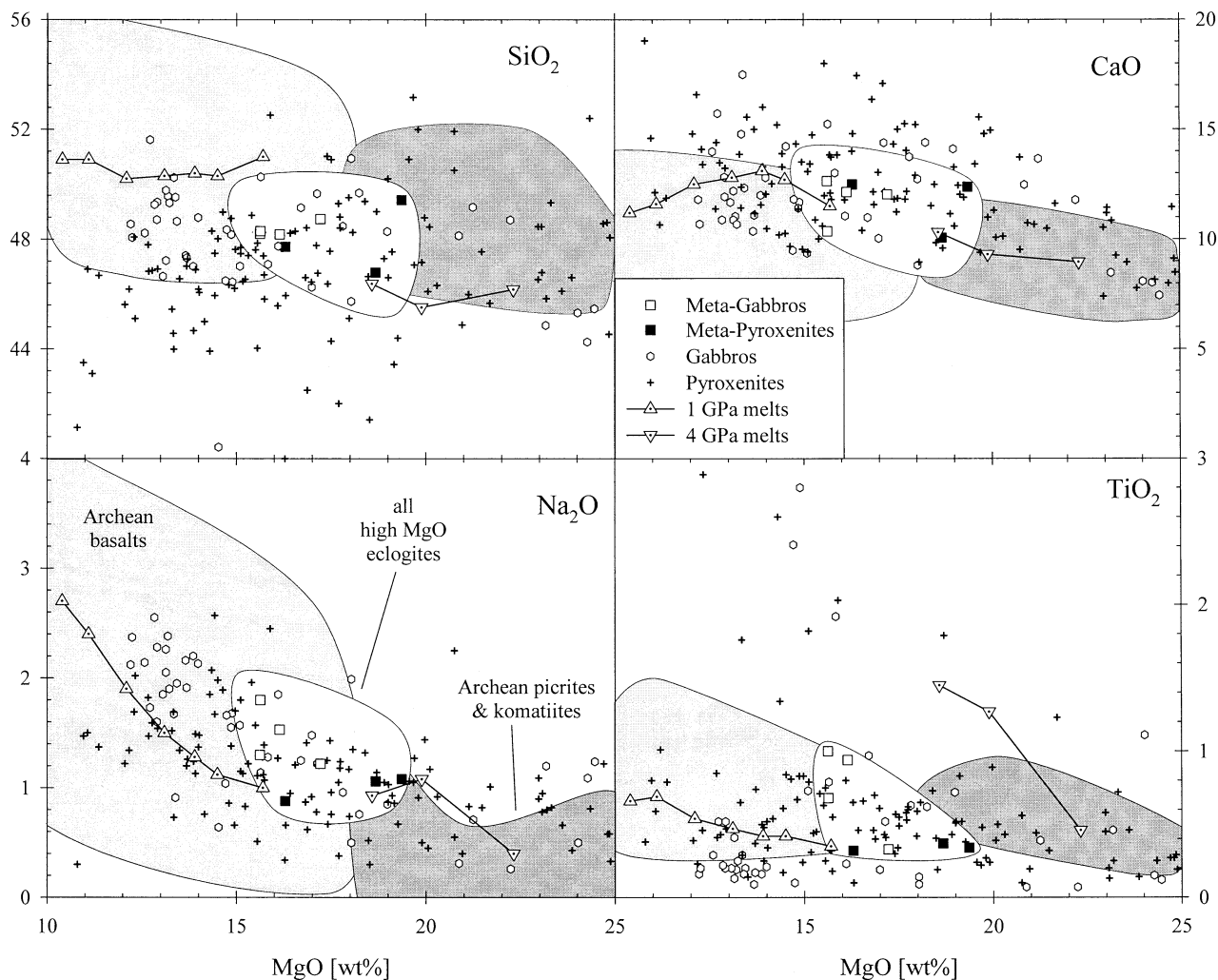
Fig. 14. Plot of SiO₂, CaO, Na₂O, and TiO₂ vs. MgO whole-rock content. Symbols and data sources as in Figure 13.

(see above). Similarly, it is unclear whether the precursors of the high MgO eclogites have been hydrothermally altered. The restricted range of oxygen isotope values suggests that the precursors either have not interacted with seawater or have coincidentally approximately normal igneous values. In the lowermost oceanic crust, hydrothermal alteration is localized along fractures and veins (Gregory and Taylor, 1981; Dick et al., 2000). Thus, it is conceivable that the precursors of the high MgO eclogites did not (or at least not extensively) interact with hydrothermal fluids. On the other hand, the "coincidence" phenomenon is a characteristic feature of seawater–hydrothermal systems. Because of $\delta^{18}O$ shifts in seawater-derived hydrothermal fluids, there is a significant range of temperatures over which the whole-rock $\delta^{18}O$ value of a gabbro that has been thoroughly hydrothermally altered in the presence of large amounts of water will, simply by coincidence, be very close to the primary magmatic value of +5.7 (Gregory and Taylor, 1981). (This "coincidence" phenomenon is absent from meteoric–hydrothermal systems as a result of the low $\delta^{18}O$ values of meteoric waters.)

Alternatively, the protoliths of the metagabbroic eclogites

could have formed by magmatic underplating of continental crust, which involves intrusion of basaltic magmas near the crust-mantle boundary. During thermal relaxation (cooling), these gabbroic rocks may be converted to mafic granulites and eclogites (Griffin et al., 1990; El Fadili and Demaiffe, 1999). Although the estimated equilibration pressures of the Koidu high MgO eclogites, in excess of 2.8 GPa, imply that these eclogites are derived from deep within the lithospheric mantle (>100 km depth), it is conceivable that the high MgO eclogites represent former crustal material that foundered or delaminated from the lower continental crust but for one reason or another, did not escape the lithosphere. The xenoliths studied by Griffin et al. (1990) and El Fadili and Demaiffe (1999) have lower MgO contents (5 to 15 wt% MgO) than the Koidu high MgO suite (16 to 20 wt% MgO). Although the depth of the transformation of gabbro to eclogite depends on bulk composition and temperature, at the estimated P-T conditions of the high MgO eclogites, all mafic to ultramafic rocks will be converted to eclogite (Green and Ringwood, 1967; Harley and Carswell, 1990).

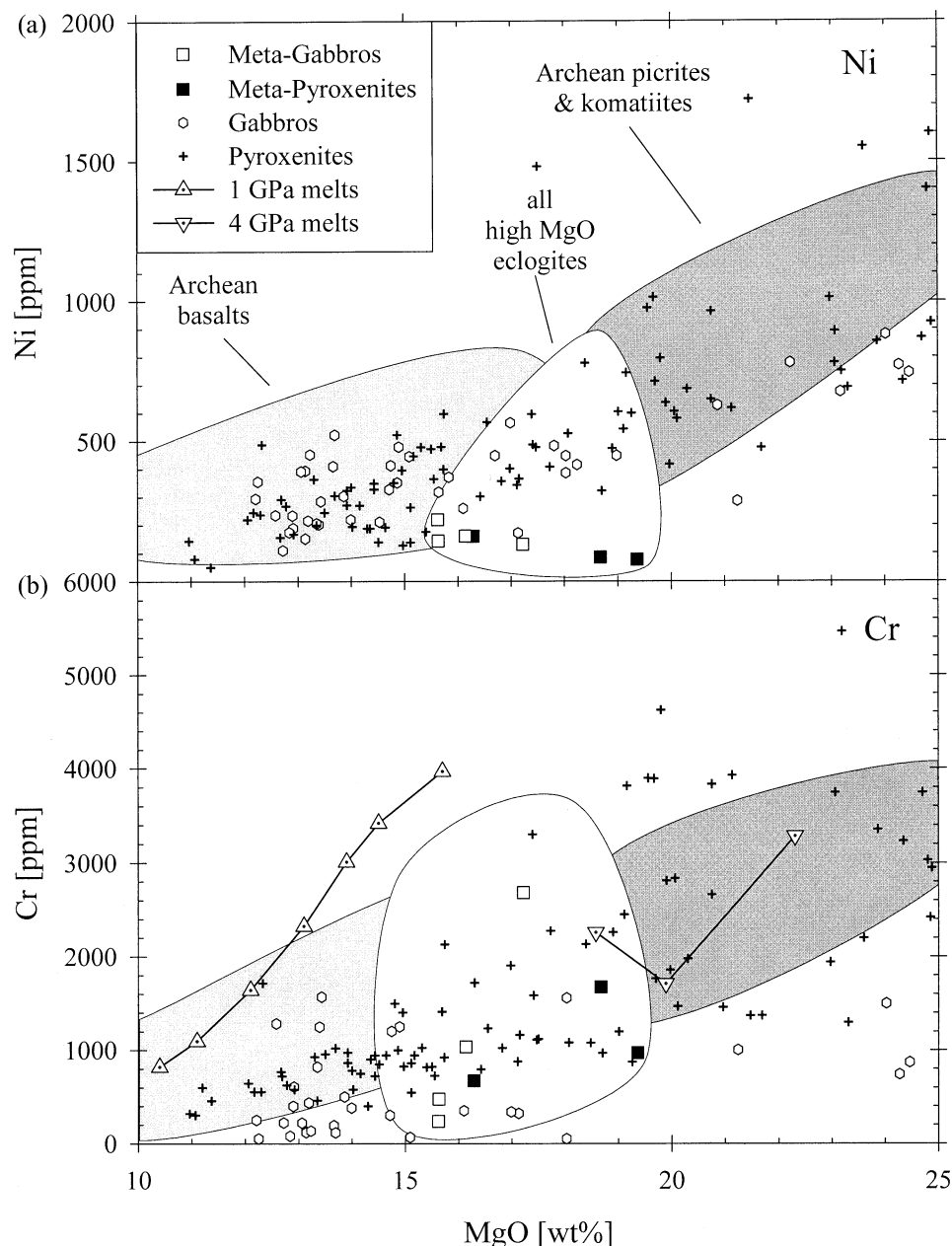The metapyroxenitic eclogites could have originated as py-

Fig. 15. Plot of Ni (a) and Cr (b) vs. whole-rock MgO content. Symbols and data sources as in Figure 13.

roxenite veins emplaced in the uppermost mantle (P < 3.3 GPa) followed by high-pressure recrystallization (P = 4.0 to 4.5 GPa) and equilibration to a normal cratonic geotherm. Mantle melting and crystallization of these mafic veins could have occurred during asthenospheric upwelling into cratonic lithosphere or in an earlier stage of a more complex history involving early shallow melting and tectonic transport to deeper levels, possibly during terrain accretion in the Archean. This proposed P-T path is qualitatively similar to the models of Kelemen et al. (1998) and Drury et al. (2001) for xenolithic and orogenic peridotites, respectively. Kelemen et al. (1998) have argued that a correlation between CaO and Yb contents in cratonic garnet peridotites implies that most melting occurred

at pressures <3 GPa, suggesting a multi-stage history may be applicable to kimberlite xenoliths. Drury et al. (2001) propose small-scale convection in the deeper part of the cratonic lithosphere induced by intrusion of diapirs as a mechanism for the emplacement of deep mantle rocks with complex metamorphic-igneous histories into cratonic lithosphere. Furthermore, Canil (2002) uses V-Al systematics in peridotites from Archean cratons to argue that these cratonic peridotites underwent melt depletion at pressures at or below 3 GPa.

If the metagabbroic high MgO eclogites represent the basal cumulate section of oceanic crust, it remains unanswered whether these eclogites are directly related to the low MgO group—that is, if both groups represent different parts of the

same slab. Although the difference in estimated equilibration temperatures suggests that the depth difference (i.e., ~25 km) between the high MgO and low MgO eclogites exceeds by far the thickness of oceanic crust, it is conceivable that the eclogites represent fragments of a dismembered or stretched slab. Conversely, the high MgO and low MgO eclogites might be derived from different slabs, comparable to the cratonic lithosphere evolution model of Helmstaedt and Schulze (1989) of stacked slabs for southern Africa.

The metapyroxenitic high MgO eclogites that originated as cumulates in the uppermost mantle are evidently unrelated to the low MgO group, which we have interpreted as originating as oceanic crust (Barth et al., 2001). If the metagabbroic eclogites are derived from underplated basalts in the lowermost continental crust, then they are also unrelated to the low MgO eclogites. These arguments point toward multiple origins of xenolithic eclogites in West Africa, as previously suggested for South African and Siberian eclogite xenoliths (Taylor and Neal, 1989; Snyder et al., 1997). Multiple origins have also been proposed for massif eclogites such as the Bohemian Massif and the Dabieshan-Sulu region, where protoliths comprise continental tholeiites, island-arc basalts, ocean-floor basalts, cumulate gabbros, and pyroxenites (e.g., Beard et al., 1992; Zhai and Cong, 1996). In these massifs, the Mg-rich and Mg-poor eclogites are genetically unrelated and crop out at different localities. Both in the Bohemian Massif and in the Dabieshan-Sulu region the Mg-rich metapyroxenitic eclogites are found in ultramafic country rocks, whereas the metabasic eclogite lenses occur in gneiss and marble. No UHP gneisses and marbles have yet been recognized in kimberlite xenolith suites.

7. CONCLUSIONS

High MgO eclogites from Pipe Number 1 of the Koidu kimberlites in Sierra Leone, Africa, have major element, trace element, and oxygen isotopic compositions distinct from the low MgO eclogites found in the same pipes. The high MgO eclogites also exhibit systematically higher equilibration temperatures than the low MgO eclogites. Thus, there is no indication that they share a common origin.

High-pressure crystal fractionation systematics and the absence of olivine and orthopyroxene suggest that the high MgO eclogites formed at lower pressures than their inferred equilibration pressures (i.e., <4 GPa). Their whole-rock major element compositions suggest a cumulate origin, generated either as garnet–pyroxene cumulates emplaced in the uppermost mantle (P < 3 GPa) or as low-pressure (crustal) plagioclase–pyroxene–olivine cumulates.

Trace element concentrations of primary minerals in the high MgO eclogites are affected by both recent and ancient metasomatism. Trace element modeling of the elements least affected by metasomatic overprinting (HREE and transition metals) suggests a low-P origin for eclogites with flat HREE patterns and a higher-P origin for eclogites with fractionated HREE. For a low-P origin two different tectonic settings are possible: the metagabbroic high MgO eclogites could represent either the basal section of oceanic crust that has been subducted or foundered mafic lower continental crust.

Associate editor: M. A. Menzies

REFERENCES

Aumento F., Melson W. G., Hall J. M., et al. (1977) Site 334. In *Initial Reports of the Deep Sea Drilling Project*, Vol. 37 (eds. F. Aumento, W. G. Melson, J. M. Hall, et al.). U.S. Government Printing Office, Washington, DC. pp. 239–287. .

Baker M. B. and Stolper E. M. (1994) Determining the composition of high-pressure mantle melts using diamond aggregates. *Geochim. Cosmochim. Acta* **58,** 2811–2827.

Barth M. G. (2001) The role of eclogites in the growth of Archean cratons: A case study from West Africa. Ph.D. thesis. Harvard University.

Barth M. G., McDonough W. F., and Rudnick R. L. (2000) Tracking the budget of Nb and Ta in the continental crust. *Chem. Geol.* **165,** 197–213.

Barth M. G., Rudnick R. L., Horn I., McDonough W. F., Spicuzza M. J., Valley J. W., and Haggerty S. E. (2001) Geochemistry of xenolithic eclogites from West Africa, Part I: A link between low MgO eclogites and Archean crust formation. *Geochim. Cosmochim. Acta* **65,** 1499–1527.

Beard B. L., Medaris G. Jr., Johnson C. M., Brueckner H. K., and Misar Z. (1992) Petrogenesis of Variscan high-temperature group A eclogites from the Moldanubian zone of the Bohemian massif, Czechoslovakia. *Contrib. Mineral. Petrol.* **111,** 468–483.

Beard B. L., Fraracci K. N., Taylor L. A., Snyder G. A., Clayton R. A., Mayeda T. K., and Sobolev N. V. (1996) Petrography and geochemistry of eclogites from the Mir kimberlite, Yakutia, Russia. *Contrib. Mineral. Petrol.* **125,** 293–310.

Bizimis M., Salters V. J. M., and Bonatti E. (2000) Trace and REE content of clinopyroxenes from supra-subduction zone peridotites. Implications for melting and enrichment processes in island arcs. *Chem. Geol.* **165,** 67–85.

Blundy J. and Wood B. (1994) Prediction of crystal-melt partition coefficients from elastic moduli. *Nature* **372,** 452–454.

Bodinier J. L., Guiraud M., Fabriès J., Dostal J., and Dupuy C. (1987) Petrogenesis of layered pyroxenites from Lherz, Freychinède and Prades ultramafic bodies (Ariège, French Pyrénées). *Geochim. Cosmochim. Acta* **51,** 279–290.

Boynton W. V. (1984) Cosmochemistry of the REE: Meteorite studies. In *REE Geochemistry* (ed. P. Henderson), pp. 63–114. Elsevier.

Canil D. (2002) Vanadium in peridotites, mantle redox and tectonic environments: Archean to present. *Earth Planet. Sci. Lett.* **195,** 75–90.

Caporuscio F. A. and Smyth J. R. (1990) Trace element crystal chemistry of mantle eclogites. *Contrib. Mineral. Petrol.* **105,** 550–561.

Coghlan R. A. N. (1990) Studies in diffusional transport: Grain boundary transport of oxygen in feldspars, diffusion of oxygen, strontium, and REEs in garnet, and thermal histories of granitic intrusions in south-central Maine using oxygen isotopes. Ph.D. thesis, Brown University.

Coleman R. G., Lee D. E., Beatty L. B., and Brannock W. W. (1965) Eclogites and eclogites: Their differences and similarities. *Geol. Soc. Am. Bull.* **76,** 483–508.

Cong B., ed. (1996) *Ultrahigh-Pressure Metamorphic Rocks in the Dabieshan-Sulu Region of China.* Kluwer.

Coplen T. B. (1996) New guidelines for reporting stable hydrogen, carbon, and oxygen isotope-ratio data. *Geochim. Cosmochim. Acta* **60,** 3359–3360.

Dawson J. B. (1984) Contrasting types of upper-mantle metasomatism. In *Kimberlites II: The Mantle and Crust–Mantle Relationships* (ed. J. Kornprobst), pp. 289–294. Elsevier.

Deines P. and Haggerty S. E. (2000) Small-scale oxygen isotope variations and petrochemistry of ultradeep (>300 km) and transition zone xenoliths. *Geochim. Cosmochim. Acta* **64,** 117–131.

Dick H. J. B., Natland J. H., Miller D. J., et al. (1999) Proceedings of the Ocean Drilling Program, Initial Reports, 176 [CD-ROM]. Available from: Ocean Drilling Program, Texas A&M University, College Station, TX 77845-9547, U.S.A.

Dick H. J. B., Natland J. H., Alt J. C., Bach W., Bideau D., Gee J. S., Haggas S., Hertogen J. G. H., Hirth G., Holm P. M., Ildefonse B., Iturrino G. J., John B. E., Kelley D. S., Kikawa E., Kingdon A., LeRoux P. J., Maeda J., Meyer P. S., Miller D. J., Naslund H. R., Niu Y.-L., Robinson P. T., Snow J., Stephen R. A., Trimby P. W., Worm H.-U., and Yoshinobu A. (2000) A long in situ section of the lower ocean crust: Results of ODP Leg 176 drilling at the Southwest Indian Ridge. *Earth Planet. Sci. Lett.* **179,** 31–51.

Drury M. R., van Roermund H. L. M., Carswell D. A., de Smet J. H., van den Berg A. P., and Vlaar N. J. (2001) Emplacement of deep upper-mantle rocks into cratonic lithosphere by convection and diapiric upwelling. *J. Petrol.* **42,** 131–140.

El Fadili S. and Demaiffe D. (1999) Petrology of eclogite and granulite nodules from the Mbuji Mayi kimberlites (Kasai, Congo): Significance of kyanite–omphacite intergrowths. In *Proceedings of the 7th International Kimberlite Conference,* Vol. 1 (eds. J. J. Gurney, J. L. Gurney, M. D. Pascoe, and S. H. Richardson), pp. 205–213. Red Roof Design.

Ellis D. J. and Green D. H. (1979) An experimental study of the effect of Ca upon garnet–clinopyroxene Fe-Mg exchange equilibria. *Contrib. Mineral. Petrol.* **71,** 13–22.

Frey F. A. (1980) The origin of pyroxenites and garnet pyroxenites from Salt Lake Crater, Oahu, Hawaii: Trace element evidence. *Am. J. Sci.* **280A,** 427–449.

Fung A. T. and Haggerty S. E. (1995) Petrography and mineral compositions of eclogites from the Koidu Kimberlite Complex, Sierra Leone. *J. Geophys. Res.* **100,** 20451–20473.

Green D. H. and Ringwood A. E. (1967) An experimental investigation of the gabbro to eclogite transformation and its petrological applications. *Geochim. Cosmochim. Acta* **31,** 767–833.

Gregory R. T. and Taylor H. P. (1981) An oxygen isotope profile in a section of Cretaceous oceanic crust, Samail ophiolite, Oman: Evidence for $\delta^{18}O$ buffering of the oceans by deep (>5 km) seawater–hydrothermal circulation at mid-ocean ridges. *J. Geophys. Res.* **86,** 2737–2755.

Griffin W. L., O'Reilly S. Y., and Stabel A. (1988) Mantle metasomatism beneath western Victoria, Australia: II. Isotopic geochemistry of Cr-diopside lherzolites and Al-augite pyroxenites. *Geochim. Cosmochim. Acta* **52,** 449–459.

Griffin W. L., O'Reilly S. Y., and Pearson N. J. (1990) Eclogite stability near the crust–mantle boundary. In *Eclogite Facies Rocks* (ed. D. A. Carswell), pp. 291–314. Blackie.

Gunn B. and Roobol M. J. (1977) Geochemistry of the igneous rocks. In *Initial reports of the Deep Sea Drilling Project,* Vol. 37 (eds. F. Aumento, W. G. Melson, J. M. Hall, et al.), pp. 735–755. U.S. Government Printing Office, Washington, DC..

Harley S. L. and Carswell D. A. (1990) Experimental studies on the stability of eclogite facies mineral parageneses. In *Eclogite Facies Rocks* (ed. D. A. Carswell), pp. 53–82. Blackie.

Harris J. W. and Gurney J. J. (1979) Inclusions in diamond. In *The properties of diamond* (ed. J. E. Field), pp. 555–591. Academic Press.

Hart S. R., Blusztajn J., Dick H. J. B., Meyer P. S., and Muehlenbachs K. (1999) The fingerprint of seawater circulation in a 500-meter section of ocean crust gabbros. *Geochim. Cosmochim. Acta* **63,** 4059–4080.

Harte B. (1987) Metasomatic events recorded in mantle xenoliths: An overview. In *Mantle Xenoliths* (ed. P. H. Nixon), pp. 625–640. Wiley.

Harte B. and Kirkley M. B. (1997) Partitioning of trace elements between clinopyroxene and garnet: Data from mantle eclogites. *Chem. Geol.* **136,** 1–24.

Hatton C. J. and Gurney J. J. (1987) Roberts Victor eclogites and their relation to the mantle. In *Mantle Xenoliths* (ed. P. H. Nixon), pp. 453–463. Wiley.

Helmstaedt H. and Doig R. (1975) Eclogite nodules from kimberlite pipes of the Colorado Plateau—Samples of subducted Franciscan-type oceanic lithosphere. *Phys. Chem. Earth.* **9,** 95–111.

Helmstaedt H. and Schulze D. J. (1989) Southern African kimberlites and their mantle sample: Implications for Archean tectonics and lithosphere evolution. In *Kimberlites and Related Rocks,* Vol. 1 (ed. J. Ross), pp. 358–368. Blackwell Scientific.

Hess P. C. (1992) Phase equilibria constraints on the origin of ocean floor basalt. In *Mantle Flow and Melt Generation at Mid-Ocean Ridges* (eds. J. Phipps Morgan, D. K. Blackman, and J. M. Sinton), pp. 67–102. American Geophysical Union.

Hills D. V. and Haggerty S. E. (1989) Petrochemistry of eclogites from the Koidu Kimberlite Complex, Sierra Leone. *Contrib. Mineral. Petrol.* **103,** 397–422.

Hodges F. N. and Papike J. J. (1976) DSDP Site 334: Magmatic cumulates from oceanic layer 3. *J. Geophys. Res.* **81,** 4135–4151.

Horn I., Rudnick R. L., and McDonough W. F. (2000) Precise elemental and isotopic ratio determination by combined solution nebulization and laser ablation ICP-MS: application to U/Pb geochronology. *Chem. Geol.* **164,** 281–301.

Hurley P. M., Fairbairn H. W., and Gaudette H. E. (1975) Progress report on early Archean Rocks in Liberia, Sierra Leone and Guayana, and their general stratigraphic setting. In *The Early History of the Earth* (ed. B. F. Windley), pp. 511–521. Wiley.

Ireland T. R., Rudnick R. L., and Spetsius Z. (1994) Trace elements in diamond inclusions from eclogites reveal link to Archean granites. *Earth Planet. Sci. Lett.* **128,** 199–213.

Irving A. J. and Green D. H. (1970) Experimental duplication on mineral assemblages in basic inclusions of the Delegate breccia pipes. *Phys. Earth Planet. Interior.* **3,** 385–389.

Jacob D., Jagoutz E., Lowry D., Mattey D., and Kudrjavtseva G. (1994) Diamondiferous eclogites from Siberia: Remnants of Archean oceanic crust. *Geochim. Cosmochim. Acta* **58,** 5195–5207.

Johnson K. T. M. (1998) Experimental determination of partition coefficients for rare earth and high-field-strength elements between clinopyroxene, garnet, and basaltic melt at high pressures. *Contrib. Mineral. Petrol.* **133,** 60–68.

Johnson K. T., Dick H. J. B., and Shimizu N. (1990) Melting in the oceanic upper mantle: An ion microprobe study of diopsides in abyssal peridotites. *J. Geophys. Res.* **95,** 2661–2678.

Johnson K. T. M. and Dick H. J. B. (1992) Open system melting and temporal and spatial variation of peridotite and basalt at the Atlantis II fracture zone. *J. Geophys. Res.* **97,** 9219–9241.

Kelemen P. B., Shimizu N., and Dunn T. (1993) Relative depletion of niobium in some arc magmas and the continental crust: Partitioning of K, Nb, La and Ce during melt/rock reaction in the upper mantle. *Earth Planet. Sci. Lett.* **120,** 111–134.

Kelemen P. B., Hart S. R., and Bernstein S. (1998) Silica enrichment in the continental upper mantle via melt/rock reaction. *Earth Planet. Sci. Lett.* **164,** 387–406.

Kohn M. J. and Valley J. W. (1998) Effects of cation substitutions in garnet and pyroxene on equilibrium oxygen isotope fractionations. *J. Metamorphic Geol.* **16,** 625–639.

Kumar N., Reisberg L., and Zindler A. (1996) A major and trace element and strontium, neodymium, and osmium isotopic study of a thick pyroxenite layer from the Beni Bousera ultramafic complex of northern Morocco. *Geochim. Cosmochim. Acta* **60,** 1429–1444.

Loubet M. and Allègre C. J. (1982) Trace elements in orogenic lherzolites reveal the complex history of the upper mantle. *Nature* **298,** 809–814.

MacFarlane A., Crow M. J., Arthurs J. W., Wilkinson A. F., and Aucott J. W. (1981) The geology and mineral resources of northern Sierra Leone. *Overseas Mem. Inst. Geol. Sci.* **7,** 103. p.

MacGregor I. D. and Carter J. L. (1970) The chemistry of clinopyroxene and garnets of eclogite and peridotite xenoliths from the Roberts Victor mine, South Africa. *Phys. Earth Planet. Interior* **3,** 391–397.

MacGregor I. D. and Manton W. I. (1986) Roberts Victor eclogites: Ancient oceanic crust. *J. Geophys. Res.* **91,** 14063–14079.

Mattey D., Lowry D., and Macpherson C. (1994) Oxygen isotope composition of mantle peridotite. *Earth Planet. Sci. Lett.* **128,** 231–241.

McCandless T. E. and Gurney J. J. (1989) Sodium in garnet and potassium in clinopyroxene: Criteria for classifying mantle eclogites.

In *Kimberlites and Related Rocks*, Vol. 2 (ed. J. Ross), pp. 827–832. Blackwell Scientific.

McDonough W. F. and Sun S.-S. (1995) Composition of the Earth. *Chem. Geol.* **120,** 223–253.

Mottana A., Carswell D. A., Chopin C., and Oberhänsli R. (1990) Eclogite facies mineral parageneses. In *Eclogite Facies Rocks* (ed. D. A. Carswell), pp. 16–52. Blackie.

Navon O. and Stolper E. (1987) Geochemical consequences of melt percolation: The upper mantle as a chromatographic column. *J. Geol.* **95,** 285–308.

Pearson D. G., Davies G. R., Nixon P. H., Greenwood P. B., and Mattey D. P. (1991) Oxygen isotope evidence for the origin of pyroxenites in the Beni Bousera peridotite massif, North Morocco: Derivation from subducted oceanic lithosphere. *Earth Planet. Sci. Lett.* **102,** 289–301.

Pearson D. G., Davies G. R., and Nixon P. H. (1993) Geochemical constraints on the petrogenesis of diamond facies pyroxenites from the Beni Bousera peridotite massif, North Morocco. *J. Petrol.* **34,** 125–172.

Rollinson H. R. (1978) Zonation of supracrustal relics in the Archaean of Sierra Leone, Liberia, Guinea and Ivory Coast. *Nature* **272,** 440–442.

Rollinson H. R. (1982) P-T conditions in coeval greenstone belts and granulites from the Archean of Sierra Leone. *Earth Planet. Sci. Lett.* **59,** 177–191.

Rollinson H. (1997) Eclogite xenoliths in west African kimberlites as residues from Archaean granitoid crust formation. *Nature* **389,** 173–176.

Rosenbaum J. M. and Mattey D. (1995) Equilibrium garnet–calcite oxygen isotope fractionation. *Geochim. Cosmochim. Acta* **59,** 2839–2842.

Rudnick R. L. and Nyblade A. A. (1999) The thickness and heat production of Archean lithosphere: Constraints from xenolith thermobarometry and surface heat flow. In *Mantle Petrology: Field Observations and High Pressure Experimentation: A Tribute to Francis R. (Joe) Boyd* (eds. Y. Fei, C. M. Bertka, and B. O. Mysen), pp. 3–12. Geochemical Society.

Rudnick R. L., Barth M., Horn I., and McDonough W. F. (2000) Rutile-bearing refractory eclogites: The missing link between continents and depleted mantle. *Science* **287,** 278–281.

Schulze D. J. and Helmstaedt H. (1988) Coesite–sanidine eclogites from kimberlite: Products of mantle fractionation or subduction? *J. Geol.* **96,** 435–443.

Schulze D. J., Valley J. W., Viljoen K. S., Stiefenhofer J., and Spicuzza M. (1997) Carbon isotope composition of graphite in mantle eclogites. *J. Geol.* **105,** 379–386.

Schulze D. J., Valley J. W., and Spicuzza M. J. (2000) Coesite eclogites from the Roberts Victor kimberlite, South Africa. *Lithos* **54,** 23–32.

Shervais J. W., Taylor L. A., Lugmair G. W., Clayton R. N., Mayeda T. K., and Korotev R. L. (1988) Early Proterozoic oceanic crust and the evolution of subcontinental mantle: Eclogites and related rocks from southern Africa. *Geol. Soc. Am. Bull.* **100,** 411–423.

Smyth J. R., Caporuscio F. A., and McCormick T. C. (1989) Mantle eclogites: Evidence of igneous fractionation in the mantle. *Earth Planet. Sci. Lett.* **93,** 133–141.

Snyder G. A., Taylor L. A., Crozaz G., Halliday A. N., Beard B. L., Sobolev V. N., and Sobolev N. V. (1997) The origins of Yakutian eclogite xenoliths. *J. Petrol.* **38,** 85–113.

Snyder G. A., Taylor L. A., Beard B. L., Crozaz G., Halliday A. N., Sobolev V. N., and Sobolev N. V. (1998) Reply to a comment by D. Jacob et al. on "The origins of Yakutian eclogite xenoliths." *J. Petrol.* **39,** 1535–1543.

Taylor L. A. and Neal C. R. (1989) Eclogites with oceanic crustal and mantle signatures from the Bellsbank kimberlite, South Africa, Part I: Mineralogy, petrography, and whole rock chemistry. *J. Geol.* **97,** 551–567.

Taylor W. R., Tompkins L. A., and Haggerty S. E. (1994) Comparative geochemistry of West African kimberlites: Evidence for a micaceous kimberlite endmember of sublithospheric origin. *Geochim. Cosmochim. Acta* **58,** 4017–4037.

Tompkins L. A. and Haggerty S. E. (1984) The Koidu Kimberlite Complex, Sierra Leone: Geological setting, petrology and mineral chemistry. In *Kimberlites, I: Kimberlites and Related Rocks*, Vol. 11A (ed. J. Kornprobst), pp. 83–105. Elsevier.

Valley J. W., Kitchen N., Kohn M. J., Niendorf C. R., and Spicuzza M. J. (1995) UWG-2, a garnet standard for oxygen isotope ratios: Strategies for high precision and accuracy with laser heating. *Geochim. Cosmochim. Acta* **59,** 5223–5231.

Walter M. J. (1998) Melting of garnet peridotite and the origin of komatiite and depleted lithosphere. *J. Petrol.* **39,** 29–60.

Wilkinson J. F. G. (1975) An Al-spinel ultramafic–mafic inclusion suite and high pressure megacrysts in an analcimite and their bearing on basaltic magma fractionation at elevated pressures. *Contrib. Mineral. Petrol.* **53,** 71–104.

Zhai M. and Cong B. (1996) Major and trace element geochemistry of eclogites and related rocks. In *Ultrahigh-Pressure Metamorphic Rocks in the Dabieshan-Sulu Region of China* (ed. B. Cong), pp. 69–89. Kluwer.

Zhang R. Y., Liou J. G., and Cong B. (1994) Petrogenesis of garnet-bearing ultramafic rocks and associated eclogites in the Su-Lu ultrahigh-P metamorphic terrane, eastern China. *J. Metamorphic Geol.* **12,** 169–186.

Zhang R., Liou J. G., and Ye K. (1996) Petrography of UHPM rocks and their country rock gneisses. In *Ultrahigh-Pressure Metamorphic Rocks in the Dabieshan-Sulu Region of China* (ed. B. Cong), pp. 49–68. Kluwer.

Zindler A. and Jagoutz E. (1988) Mantle cryptology. *Geochim. Cosmochim. Acta* **52,** 319–333.